UiT
NORGES
ARKTISKE
UNIVERSITET

INSTITUTT FOR FARMASI

Advanced Drug Delivery System for New Chemical Entity Destined for Wound Therapy:

Anti-biofilm Potential of Novel Drug Delivery System

—

Ida Emilie Thoresen

Masteroppgave i Farmasi, Mai 2014

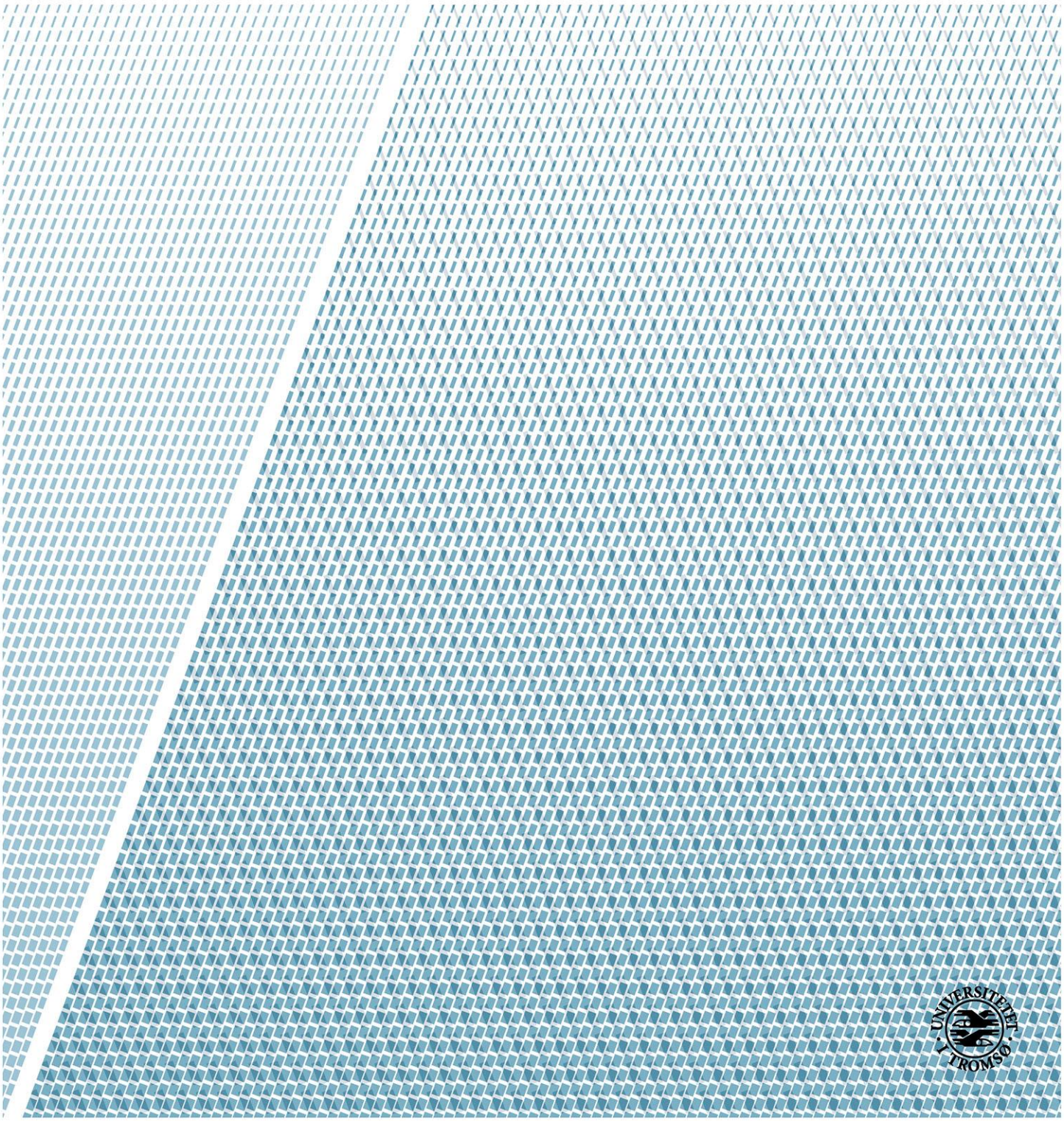

MASTER THESIS FOR THE DEGREE MASTER OF PHARMACY

ADVANCED DRUG DELIVERY SYSTEM FOR NEW CHEMICAL ENTITY DESTINED FOR WOUND THERAPY:

ANTI-BIOFILM POTENTIAL OF NOVEL DRUG DELIVERY SYSTEM

BY

IDA EMILIE THORESEN

MAY 2014

SUPERVISORS

Professor Nataša Škalko-Basnet

and

Gry Stensrud, Vice President Technical Development and Operations, Photocure ASA

Drug Transport and Delivery Research Group

Department of Pharmacy

Faculty of Health Sciences

University of Tromsø – The Arctic University of Norway

Acknowledgement

The present work was carried out at the Drug Transport and Delivery Research Group, Department of Pharmacy, University of Tromsø – The Arctic University of Norway, Norway from October 2013 to May 2014.

First, I want to express my gratitude to my supervisor Professor Nataša Škalko-Basnet for excellent guidance. You have always had the time for small discussions. Your encouragement has inspired me, and your expertise has opened my mind to the world of pharmaceutics. Thank you for sharing your knowledge and for believing in me during this period!

Many thanks to my other supervisor Gry Stensrud at Photocure ASA, for good collaboration. Thank you, Gry and Photocure ASA, for trusting me this assignment! You have opened my eyes to a new field of medical science!

Thanks to Chitinor AS for providing the chitosan used during this study.

Thanks to my fellow master student Muna Hadafow. We started this study together, and although we went separate ways half way through the study, we could always discuss and compare results.

Big thanks to Julia Maria Kloos for your patience and cooperation during my time in the microbiology laboratory. You were always there when I needed, and you always had time to help. Thank you for showing me the world of microbiology!

Thanks to Professor Kaare Nielsen, PI for Research group in microbiology, molecular and pharmaco-epidemiology, for helpful advices!

Thanks to Janne Stangeland for your technical expertise and for always finding time to help, especially with equipment and the HPLC machine.

Thanks to PhD student Ekaterina Mishchenko at Norwegian College of Fishery Science for sharing your expertise and knowledge about biofilms. You were very helpful!

I would also like to thank my fellow students at Department of Pharmacy for making these five years memorable. Very special thanks to Malin for all the good times together in the laboratory and at the reading room, especially this last year. I will miss you!

Sincerely thanks to my family for always believing in me. I will always be grateful for the support you have shown me throughout these five years I have been living in Tromsø!

-Ida Emilie Thoresen, May 2014

Table of contents

List of Figures

List of Tables

Abstract

Damage to the healthy skin barrier leads to a rapid and complex process of wound healing to restore the skins normal function and structure. The presence of bacteria in wounds such as pressure ulcers and diabetic foot ulcers impairs the healing process and leads to increased patient morbidity and mortality as well as reduced patient life quality. Bacteria growing in the wound environment form biofilm, a thick hydrophobic matrix that provides an optimal environment for bacterial survival. In recent years, an increase of bacterial resistance against antibiotics existing on the market today has led to the development of new treatment options such as e.g. antimicrobial photodynamic therapy (PDT).

Lecithin/chitosan nanoparticles containing a New Chemical Entity (NCE) were prepared and characterized for their size distribution and zeta potential. Entrapment of NCE in nanoparticles was approximately 23 %. The nanoparticles exhibited a bimodal size distribution with a representative size of around 250 nm. The overall surface charge was found to be slightly positive. A method for evaluating elimination *Staphylococcus epidermidis* biofilm after the treatment with NCE-mediated PDT was optimized throughout this project. During biofilm elimination, NCE in both free form and entrapped in nanoparticles were applied to the biofilm prior to the light irradiation. NCE concentrations of 0.01, 0.1 and 1 mM were found to be safe for use, a light dose of both 37 and 90 J/cm^2 were found to be applicable, and treatment intervals of 6 and 24 hours with NCE prior to light irradiation were used. The effect of NCE on biofilm without light exposure was also evaluated. Vancomycin was used as a standard positive control during the entire experimental period. The results indicated a very small reduction of intact biofilm after the treatment with NCE-mediated PDT under optimal growth conditions for *S. epidermidis*. Moreover, biofilm reduction was also observed after treatment with NCE alone.

Although the results exhibited minimal biofilm reduction after PDT treatment, this study indicate that NCE-mediated PDT has the potential to be a new optional treatment against biofilm-forming bacteria that colonizes chronic wounds. Further optimization of the elimination method is necessary, and highly interesting.

Keywords: bacterial biofilm, antimicrobial photodynamic therapy, lecithin/chitosan nanoparticles

Abstract (Norwegian)

Når huden blir skadet, starter en rask og kompleks sårhelingsprosess som har som mål å gjenopprette hudens normale struktur og funksjon. Bakterier som er tilstede i sår, som for eksempel trykksår og fotsår hos diabetikere, svekker sårhelingsprosessen i tillegg til å føre til økt sykelighet og dødelighet, og redusert livskvalitet, hos pasienten. Bakteriene som lever i et sår danner en såkalt biofilm, en hydrofobisk matriks som sørger for et optimalt vekstmiljø slik at bakteriene kan overleve. I de senere år har andelen antibiotikaresistente bakterier vokst, noe som har ført til en utvikling av nye behandlingsalternativer. Antimikrobiell fotodynamisk terapi (photodynamic therapy; PDT) er en av disse nye alternativene.

Nanopartikler laget av lecitin og kitosan som inneholder en ny kjemisk enhet (New Chemical Entity; NCE) ble laget, og deres størrelsesdistribusjon og overflateladning ble karakterisert. Mengden NCE inkorporert i nanopartiklene var omtrent 23 %. Nanopartiklene hadde en bimodal størrelsesdistribusjon med en representativ størrelse på omtrent 250 nm, mens overflateladningen var svakt positiv. En metode for å evaluere eliminasjon av *Staphylococcus epidermidis* biofilm etter behandling med NCE-mediert PDT ble optimalisert gjennom hele prosjektet. NCE i både fri form og inkorporert i nanopartikler ble testet på biofilmen. Effekten av NCE uten lyseksponering ble også undersøkt. NCE konsentrasjonene 0,01, 0,1 og 1 mM viste en sikker bruk med tanke på toksisitet, lysdoser på både 37 og 90 J/cm^2 var anvendbare, og behandlingstider på både 6 og 24 timer før eksponering for lys ble brukt. Vankomycin ble brukt som en standard positiv kontroll under hele den eksperimentelle perioden. Resultatene indikerte en svært liten reduksjon av den intakte biofilmen etter behandling med NCE og lyseksponering under optimale vekstforhold for *S. epidermidis*. I tillegg, reduksjon av biofilm ble også observert etter behandling med kun NCE.

Selv om resultatene foreviste en minimal reduksjon av biofilm etter behandling med PDT, viser denne studien at NCE-mediert PDT har potensiale til å bli et nytt behandlingsalternativ for bakterier som danner biofilm i kroniske sår. Videre optimalisering av metoden er nødvendig og svært interessevekkende.

Nøkkelord: bakteriell biofilm, antimikrobiell fotodynamisk terapi, lecitin/kitosan nanopartikler

List of Abbreviations

5-ALA/ALA	5-aminolevulinic acid
AK	Actinic keratosis
ALAS	5-aminolevulinate synthase
APDT	Antimicrobial photodynamic therapy
BCC	Basal cell carcinoma
BMV	Betamethasone valerate
CFU	Colony forming units
CP	Clobetasol-17-propionate
CV	Crystal violet, 0.1 %
DD	Degree of deacetylation
DFV	Diflucortolone valerate
DLS	Dynamic light scattering
DNA	Deoxyribonucleic acid
EE	Entrapment efficiency
EPSs	Extracellular polymeric substances
HAL	Hexylaminolevulinate
HPLC	High performance liquid chromatography
LAF	Laminar airflow
LCNPs	Lecithin/chitosan nanoparticles
LD_{50}	Lethal dose causing death in 50 % of population
LED	Light-emitting diode
MAL	Methylaminolevulinate
MIC	Minimum inhibitory concentration
MRSA	Methicillin-resistant *Staphylococcus aureus*
MRSE	Methicillin-resistant *Staphylococcus epidermidis*
MW	Molecular weight
NCE	New chemical entity
NMFs	Natural moisturizing factors
NMIBC	Non-muscle invasive bladder cancer

NO	Nitric oxide
NPs	Nanoparticles
OD	Optical density
OD_{600}	Optical density at 600 nm
PBS	Phosphate-buffered saline
PCS	Photon correlation spectroscopy
PDT	Photodynamic therapy
PDTA	Photodynamic therapy agent
PI	Polydispersity index
PLGA	Poly(lactic-co-glycolic acid)
PpIX	Protoporphyrin IX
PROTOS III	Protoporphyrinogen III
PS	Photosensitizer
QS	Quorum sensing
ROS	Reactive oxygen species
RT	Room temperature
SC	*Stratum corneum*
SD	Standard deviation
TBO	Toluidine blue O
TEWL	Transepidermal water loss
TSA	Tryptic soy agar
TSB	Tryptic soy broth
TSB1%glu	Tryptic soy broth containing 1 % glucose
ZP	Zeta potential

1. General Introduction

The healthy skin is a barrier that protects the body from environmental dangers such as toxic chemicals, ultraviolet radiation and mechanical trauma in addition to regulate the body temperature and prevent water and electrolyte loss (Sherwood, 2010; Hwa et al., 2011). The skin also harbors a rich and diverse community of microorganisms that prevents the invasion of opportunistic/pathogenic organisms (Christensen and Brüggemann, 2014). When the skin is injured, the barrier loses its normal function and structure, initiating a complex biological process of wound healing (Shaw and Martin, 2009). A wound can be classified as either acute or chronic, depending on the wound healing process. Chronic wounds displays a slow healing process that fails to heal due to factors such as patient malignancies, poor primary treatment and persistent infections. The healing process of chronic wounds can be severely impaired when pathogenic bacteria such as e.g. *Staphylococcus aureus* and *Pseudomonas aeruginosa* are present (Boateng et al., 2008), increasing the risk of patient morbidity and mortality.

When pathogenic bacteria critically colonize wounds, they aggregate and form communities within a matrix comprised of proteins, polysaccharides and lipids, known as biofilm. Bacteria grown in biofilms are more resistant to the hosts immune response and environmental exposures such as antimicrobial agents (Thomson, 2011; Demidova-Rice et al., 2012).

A proper wound management includes a significant reduction in bioburden of the wound bed by creating conditions in the wound that are unfavorable for the bacteria (Bowler, 2002; Edwards and Harding, 2004). The use of topical antibiotics can help reduce the wound's bioburden, but a rapid emerge of antibiotic resistance due to bacterial gene mutations and biofilm-formation have forced scientists to find new options for antibacterial treatment. Photodynamic therapy (PDT) is one of these optional treatments, exhibiting several favorable features such as broad-spectrum of action, lack of PDT resistance and equal killing effectiveness (Jori et al., 2006; Dai et al., 2009). Treatment with PDT involves the combination of a light-sensitive molecule, oxygen and visible light, resulting in apoptotic and necrotic cell death. For optimal effect and increased biological and chemical stability, the photodynamic therapy agent can be entrapped in e.g. nanoparticles (NPs) (Bechet et al., 2008).

The selected PDT agent in our project was New Chemical Entity (NCE), recently developed and patented by Photocure ASA. NCE is a derivative of the naturally occurring haem precursor 5-aminolevulinic acid. Encapsulation of the PDT agent gives rise to several advantages

regarding treatment of bacterial infections such as reduced drug resistance, improved selectivity and non-toxicity (Hamblin and Hasan, 2004).

In this study, nanoparticles made of lecithin and chitosan were used due to their biocompatibility and biodegradability. Chitosan, a natural polycationic polysaccharide, has characteristics that enable its antimicrobial action through several mechanisms of action (Pelgrift and Friedman, 2013).

2. Introduction

2.1. Skin

The skin is the largest organ of the body. The most important function of the skin is to create an effective barrier that protects the body from the environment, e.g. foreign pathogens and chemical/physical exposures (Proksch et al., 2008; Sherwood, 2010). Human skin consist of two layers, namely epidermis and dermis, protected by the *stratum corneum* (Bouwstra and Ponec, 2006; Sherwood, 2010).

2.1.1. Skin structure

The epidermis is a viable layer underlying the *stratum corneum* (SC) (Bouwstra and Ponec, 2006). The epidermis has a thickness of approximately 50-100 µm and consists of various layers (**Figure 1**). These layers are, from the inside to the outside, the *stratum basale* (basal layer), the *stratum spinosum* (spinous layer) and the *stratum granulosum* (granular layer) (El Maghraby et al., 2008; Baroni et al., 2012). The SC consist of dead and flattened cells called corneocytes (Bouwstra and Ponec, 2006). The loss of these cells from the surface is balanced by cell growth in the inner epidermal layers. Cells in the inner epidermal layers, called keratinocytes, are cuble-like shaped in addition to be living and rapidly dividing (Sherwood, 2010). The epidermis has no vascular network, thereof the cells get nutrition through diffusion from a rich vascular network found in the underlying dermis. As the epidermal layer is constantly renewing, the newly formed cells push the older cells closer to the surface and away from the nutrition, causing the older cells to become flattened and die. When the keratinocytes die, they start to undergo different changes in both structure and composition, resulting in a transformation into corneocytes filled with keratin filaments and water. The corneocytes provides, together with an intercellular lipid-rich matrix, a tough and protective keratinized layer, referred to as the SC (Bouwstra and Ponec, 2006; Sherwood, 2010). The thickness of this keratinized layer differs (10-20 µm), depending on the different regions of the body and the pressure the skin is subjected to. The keratinized layer is capable of resisting the loss of water to the environment in addition to prevent penetration of foreign material into the body (Sherwood, 2010; Hwa et al., 2011).

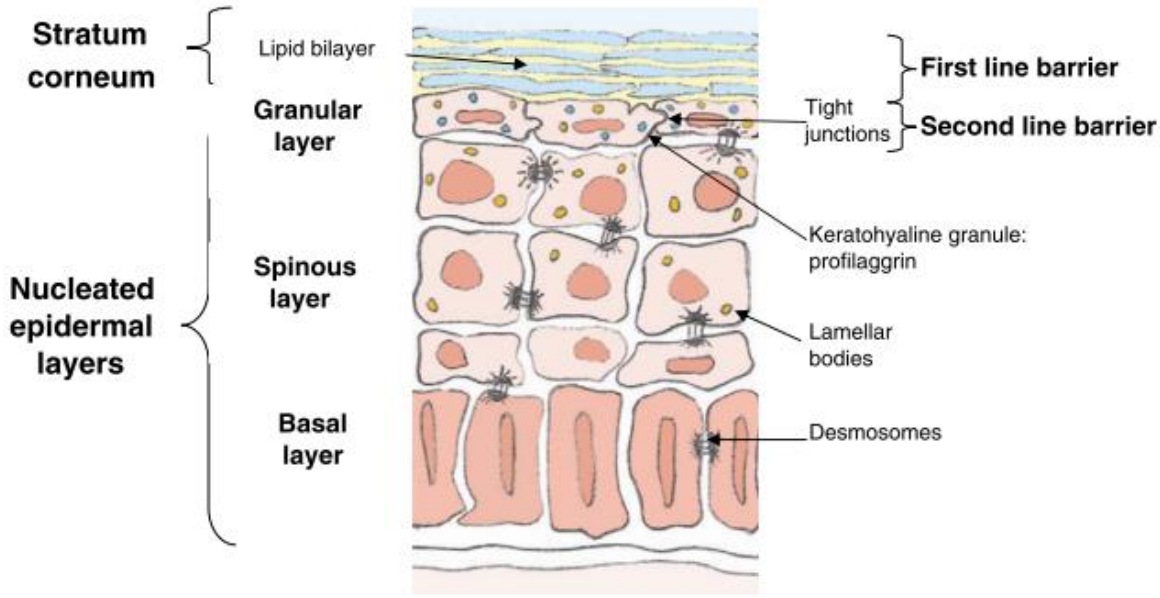

Figure 1: Epidermal structure and differentiation (Baroni et al., 2012).

The dermis (**Figure 2**), underlying the epidermis with a thickness of 1-5 mm, is a connective tissue consisting of elastin and collagen fibers in a glycosaminoglycan gel in addition to blood and lymphatic vessels and nerve endings (El Maghraby et al., 2008; Sherwood, 2010; Hwa et al., 2011). The elastin fibers provide the stretch and the collagen fibers strength. The dermal blood vessels supply blood to the epidermal and dermal layers in addition to playing a role in temperature regulation and heat exchange between the skin surface and the surrounding external environment. Afferent nerve endings detect somatosensory inputs like e.g. pressure, pain and temperature, while efferent nerve endings controls hair erection, gland secretion and blood vessel caliber (related to heat exchange). The skin has three appendages rooted in the dermis, namely sweat glands, sebaceous glands and hair follicles. Sweat glands are distributed over most of the body, helping the skin to cool and regulate the temperature by excretion and evaporation of dilute salt solutions. Sebaceous glands produce an oily secretion called sebum. Sebum oils both the outer keratinized skin layer and the hairs, making them waterproof and preventing them from drying and cracking. The sebaceous glands connect to the hair follicles, forming the pilosebaceous unit. The hair follicles secrete keratin and other proteins, forming the hair shaft. Hairs on the skin surface make the skin more sensitive to tactile stimuli i.e. touch (Sherwood, 2010; Sanford and Gallo, 2013).

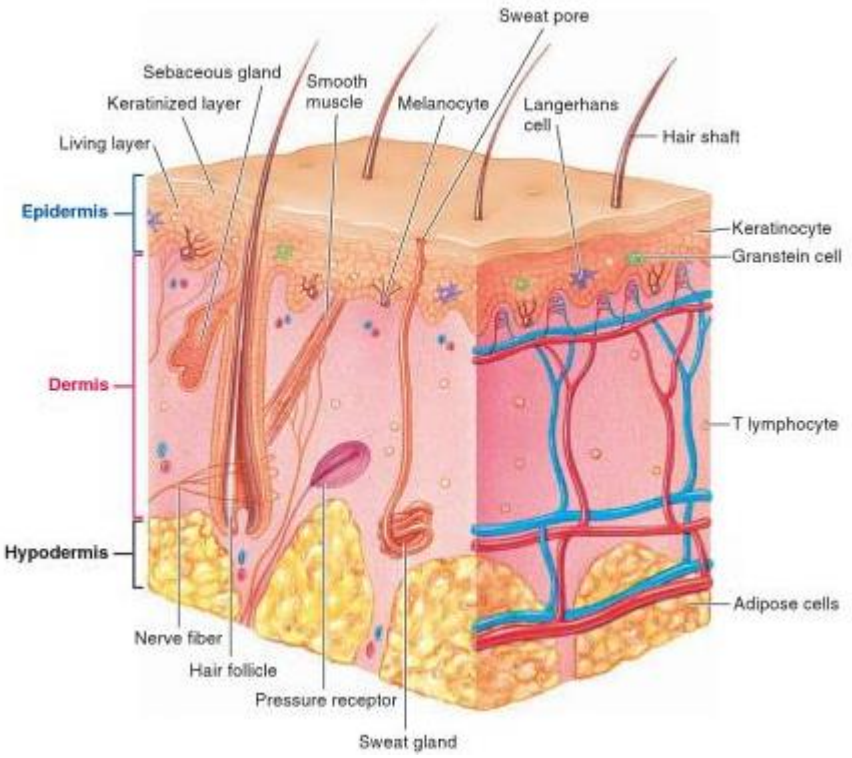

Figure 2: Structure of the skin showing the epidermis, dermis and hypodermis (Sherwood, 2010).

The skin is connected to underlying tissue such as bone or muscle through hypodermis (**Figure 2**) (Sherwood, 2010). The hypodermis is a connective tissue, consisting mostly of fat cells, also known as adipose tissue. Hypodermis functions as energy storage, insulation and protective padding (Hwa et al., 2011).

2.1.2. The healthy skin barrier

The most important role of the skin barrier is to prevent extensive water loss and to protect against environmental threats like toxic chemicals, ultraviolet radiation, microorganisms and mechanical trauma (Proksch et al., 2008; Hwa et al., 2011). In addition, the skin is a sensory organ and the primary regulator of body temperature (Lee et al., 2006). To serve as a primary defense system, the skin has to be healthy and the barrier intact.

The intact skin barrier is a collective term for individual barrier responsibilities, largely confined to the SC (Rosso and Cash, 2013). These include the permeability, antimicrobial, immune response and photo-protection barriers. The most important barrier is the permeability barrier, which controls the epidermal water flux and substance permeation. Another important

factor for the epidermal permeability barrier is the acidity of the SC, with a pH ranging from 4.5 to 5.5 (Lee et al., 2006).

The heterogeneous arrangement of the SC is often compared to "bricks and mortar" (**Figure 3**) (El Maghraby et al., 2008; Hwa et al., 2011). In this arrangement, the corneocytes act like hydrophilic "bricks" and intercellular lipid matrix acts like hydrophobic "mortar". The intercellular lipid matrix consists of three types of lipids, namely ceramides, cholesterol and free fatty acids, arranged as multiple bilayers. This intercellular lipid matrix plays an important role in the skin barrier function by aiding in the prevention of internal water loss and permeation of water-soluble molecules due to its hydrophobicity.

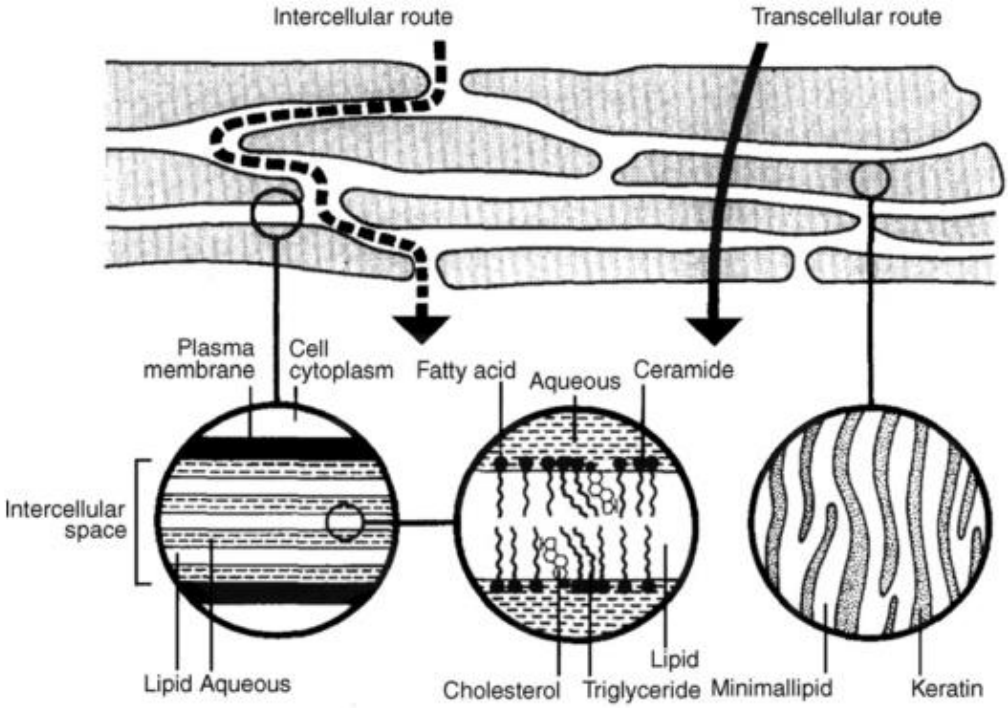

Figure 3: Model of the *stratum corneum* showing the "bricks and mortar" arrangement. Also shown are the two routes for transepidermal pathway of molecules through intact *stratum corneum*; the intercellular route and the transcellular route (El Maghraby et al., 2008).

Molecules applied to the skin can permeate the skin through two main routes, namely (a) the transappendageal pathway, and (b) the transepidermal pathway (El Maghraby et al., 2008).

The transappendageal pathway includes the permeation across the hair follicles and through the sweat glands, directly opened into the skin surface environment (El Maghraby et al., 2008).

The transepidermal pathway includes permeation across the healthy SC, and can be further divided into the intercellular route, as the predominant route, and the transcellular route (Hadgraft, 2004; El Maghraby et al., 2008). The intercellular route is permeation through the intercellular lipid matrix while the transcellular route is permeation through both the corneocytes and the intercellular lipid matrix (**Figure 3**).

All molecules permeate the skin using a combination of the different pathways, depending on their physicochemical properties (El Maghraby et al., 2008).

2.1.3. The microbiota of healthy skin

In addition to act as a protective barrier, the skin harbors a rich and diverse community of microorganisms, referred to as the skin microbiota (Hannigan and Grice, 2013). Microorganisms such as bacteria, fungi, viruses, archaea and microeukaryotes inhabit various environments in the body, e.g. skin, gut and oral cavity.

The skin is a complex ecosystem with special environmental conditions (Hannigan and Grice, 2013). At the skin surface, the temperature is cooler than the core body temperature, the skin is slightly acidic and the skin surface is continuously renewing due to rapid cell proliferation and differentiation of the epidermal layer. Environmental niches like this result in a selective microbial colonization of the skin surface. An important role of the skin microbiota is to act as a "colonization resistance", blocking the colonization and/or invasion of pathogenic or opportunistic organisms by occupation of distinct environmental niches. The stability of the skin microbiota is a balance between the human host defense mechanisms and the properties of the microbial inhabitants (Christensen and Brüggemann, 2014).

The skin microbiota varies depending on the human skin topography, but the most abundant bacterial genera found on human skin layers are *Staphylococcus*, *Propionibacterium*, *Micrococcus* and *Cyronebacterium* (Christensen and Brüggemann, 2014). *Staphylococcus epidermidis* is predominant on human epithelia whilst *Propionibacterium acnes* is predominant in the pilosebaceous units (Christensen and Brüggemann, 2014).

2.1.4. The impaired skin barrier

With an impairment of the skin barrier, hence the SC, the skin hydration decreases due to increased transepidermal water loss (TEWL), leading to a disruption in the homeostatic water gradient within the epidermis (Rosso and Cash, 2013). Further, TEWL will lead to impaired functions of water-dependent enzymes important for normal epidermal cell proliferation and differentiation. Water-dependent enzymes are also involved in the maintenance of the normal SC structure. The epidermis has a self-repair mechanism in case of increased TEWL, restoring and maintaining the permeability barrier of the SC. This mechanism includes the release of stored lipids in the lower SC in addition to increased water retention by increased production of natural moisturizing factors (NMFs). Another consequence of increased TEWL is the increased production of proinflammatory cytokines, leading to inflammation and epidermal hyperproliferation. In case of persistent increase of TEWL without self-repair of the SC, the skin barrier loses its normal function and structure, giving rise to visible dryness, decreased skin elasticity and resiliency, fissuring, hyperkeratosis and erythema secondary to inflammation (Rosso and Cash, 2013).

2.2. Wounds

Skin wounds are a result of "disruption of normal anatomic structure and function" due to defects or breaks in the skin or underlying physiological or medical conditions (Lazarus et al., 1994; Boateng et al., 2008). Wounds are classified as either acute or chronic (Lazarus et al., 1994; Boateng et al., 2008; Singh et al., 2013). Acute wounds are wounds that completely heals within 8-12 weeks and with minimal scarring, e.g. bite wounds, puncture wounds, abrasions and burns (Singh et al., 2013). Acute wound healing follows the normal wound healing and repair process described in more detail later. Chronic wounds are tissue injuries that slowly heal, with a healing period of minimum 12 weeks, e.g. pressure ulcers, diabetic foot ulcers, ischemic wounds and venous insufficiency ulcers (Singh et al., 2013). Chronic wounds fail to heal and are often reoccurring due to persistent infections, diabetes and other malignancies, poor primary treatment and other factors related to the patient (Boateng et al., 2008).

Based on the types of skin layers and the skin area affected, a skin wound can also be classified as either (a) a superficial wound, (b) a partial thickness wound, or (c) a full thickness wound (Boateng et al., 2008).

Superficial wounds are wounds caused by injury to the epidermal skin surface.

Partial thickness wounds are wounds caused by injury that affects both the epidermis and dermis in addition to blood vessels, sweat glands and pilosebaceous units.

Full thickness wounds are wounds caused by injury that affects the epidermis, dermis and the hypodermis. Deeper tissue underlying the hypodermis can also be affected (Boateng et al., 2008).

2.2.1. Wound healing

Wound healing is a function involving rapid and functional production of skin layers and appendages that physiologically fits as native skin (Mohd Hilmi et al., 2013). The complex biological process of skin wound healing involves both molecular, cellular and humoral responses (Reinke and Sorg, 2012). These responses are dynamic and highly regulated mechanisms that begin right after skin wounding and might last for years. The closure of a skin wound can be by either regeneration or repair. Regeneration of skin is described by specific substitution of tissue while skin repair is described by an unspecific healing involving fibrosis and scar formation (Reinke and Sorg, 2012).

2.2.1.1. Wound repair

Wound repair can be divided into four phases, overlapping in time and space, based on different biological process, namely (a) the immediate response phase, (b) the inflammatory response phase, (c) the proliferative phase, and (d) the remodeling phase (Reinke and Sorg, 2012; Shaw and Martin, 2009).

The immediate response phase starts with an abundance of damaging signals (**Figure 4**). As a response to skin injury, damaged and stressed cells activates a signaling pathway, leading to a phosphorylation cascade of signaling molecules. This cascade ends with cellular changes that include alterations in cell survival, metabolism and gene expression. The injured skin also sends out clotting factors, initiating a clotting cascade resulting in vasoconstriction and formation of a provisional matrix comprised of cytokines, growth factors and fibrin. The blood clot stops local hemorrhage and fills the tissue gap in addition to act as a scaffold structure for the migration of endothelial cells, leukocytes, keratinocytes and fibroblasts (Shaw and Martin, 2009; Reinke and Sorg, 2012).

The inflammatory response phase is activated during the immediate response phase with a leak of leukocytes from damaged blood vessels (**Figure 4**). The leukocytes act as a chemoattractant, attracting neutrophils and macrophages from nearby vessels. The neutrophils release mediators that amplifies the inflammatory response in addition to clean the wound by excreting antimicrobial substances (cationic peptides) and proteinases. The macrophages perform phagocytosis of cell debris and pathogens. The inflammatory response phase is further enhanced by vessel dilation and increased vascular permeation triggered by nitric oxide (NO), histamine and other factors (Shaw and Martin, 2009; Reinke and Sorg, 2012).

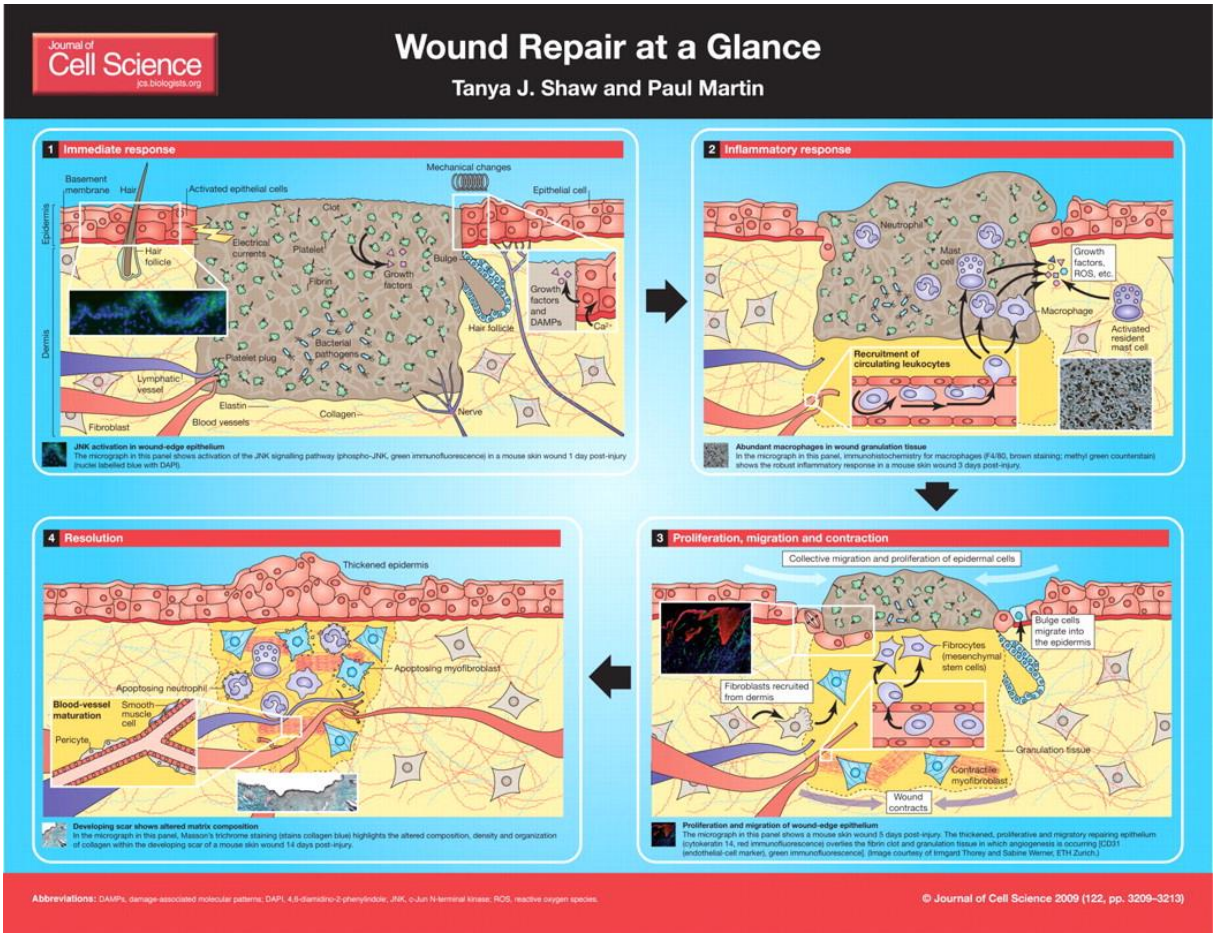

Figure 4: Wound repair at a glance (Shaw and Martin, 2009).

The proliferative phase is important for closing of the wound. Epithelial cells and fibroblasts replace the blood clot formed during the immediate response phase (**Figure 4**). The re-epithelialization process is performed by keratinocytes, and takes place at the wound edges in the epidermis. The blood clot is replaced by granulation tissue, a network consisting mostly of

collagen synthesized from fibroblasts and myofibroblasts. Formation of new blood vessels, angiogenesis, provides oxygen and nutrients to the growing tissues and assists the formation of granulation tissue. Repair of lymph vessels, lymphangiogenesis, takes care of accumulated fluid (Shaw and Martin, 2009; Reinke and Sorg, 2012).

The remodeling phase is essential in the wound healing process for the restoration of fully functional tissue in addition to a "normal" appearance. The epidermal sheet does not return to its pre-wound state due to lack of subepidermal appendages such as the sweat glands and the pilosebaceous units. The normal architecture of the dermis is accomplished by equilibrium of collagen synthesis, bundling and degradation (**Figure 4**). The blood vessels are refined and matured to a functional network. The acute metabolic activity that responded to skin injury slows down and eventually stops. An imperfect regulation of wound remodeling can lead to excessive scar formation (Shaw and Martin, 2009; Reinke and Sorg, 2012).

Nutrients (e.g. proteins, fatty acids, vitamin C, zinc and iron), blood cells, oxygen and wound exudate are important components in the complete wound healing process (Boateng et al., 2008; Wild et al., 2010). The wound exudate is described as blood without red cells and platelets, and its function is to keep the wound moist in addition to irrigate it. A moist wound bed is essential for effective wound healing, giving an ideal environment for epithelial cell migration and mitosis. The wound exudate also supplies the wound with nutrients and leukocytes (Boateng et al., 2008).

Delays in the wound healing process, resulting in a chronic wound, can be influenced by many different factors such as drugs, diseases, age, oxygen supply, pressure, temperature, application of wound dressings, wound exudate and the presence of microbial antigens (Singh et al., 2013).

2.2.2. Bacterial wound infections

In dermal wounds, the skin becomes more susceptible to microorganisms developing communities on the wound surface and within the wound environment, causing a delay in the wound healing process (Thomson, 2011; Demidova-Rice et al., 2012). In addition, a bacterial infection contributes to wound chronicity and increased risk of patient morbidity and mortality (Demidova-Rice et al., 2012; Vecchio et al., 2013). The presence of bacteria in a wound induces an excessive inflammatory response. The recruitment of more inflammatory cells leads to a production of several proteases that degrades growth factors and granulation tissue within the

wound, resulting in tissue damage. Bacteria also produce these proteases (Demidova-Rice et al., 2012).

Depending on the extent of microbial infestation and necessary treatment, the presence of a bacterial burden in chronic wounds can be classified as either (a) contamination, (b) colonization, (c) critical colonization, or (d) infection, respectively (Singh et al., 2013).

Contamination: a normal condition in a chronic wound that does not delay or impair the healing process. Involves the presence of non-replicating bacteria.

Colonization: the presence of replicating bacteria that colonize and contaminate without a host reaction. The bacterial colonization does not delay or impair the healing process.

Critical colonization: local tissue damage due to the presence of replicating bacteria that may contribute to a delay in the healing process.

Infection: bacterial tissue invasion that leads to impaired and delayed healing. The replicating bacteria causes a host reaction (Singh et al., 2013).

The most common bacteria that colonizes a wound include *Pseudomonas aeruginosa*, *Staphylococcus epidermidis*, *Staphylococcus aureus*, *Enterococcus faecalis* and *Acinetobacter baumannii* (Percival et al., 2012). Bacteria that critically colonizes chronic wounds are often forming communities called biofilm (Demidova-Rice et al., 2012).

2.2.2.1. Bacterial biofilm

A bacterial biofilm consists of bacteria that grows and encases themselves within a matrix of extracellular polymeric substances (EPSs) composed of proteins, lipids, polysaccharides and extracellular bacterial DNA (Percival et al., 2012; Taraszkiewicz et al., 2012). Biofilms can grow on both biologic and non-biologic surfaces, comprising of either a single microbial species or multiple microbial species (O'Toole et al., 2000). Biofilms comprising of a single microbial species predominates in infections and on the surface of medical implants, while biofilms comprising of multiple microbial species often predominates in the environments.

Biofilm formation (**Figure 5**) starts with an initial, reversible attachment of planktonic bacteria to a biological surface (Hall et al., 2014). Further, the adherent bacteria multiply, the surface attachment gets stronger and the bacteria begins to differentiate, initiating a complex and

organized process of biofilm genesis. Following surface attachment, adherent cells up-regulates a process termed "quorum sensing" (QS), a communication between biofilm-forming bacteria that regulates the cooperative activities and physiological processes. Maturation of biofilm occurs through processes such as nutrient consumption, up-regulation of virulence factors, secretion of EPSs forming the biofilm matrix and recruitment of other bacterial species or mammalian cells (e.g. platelets). When the biofilm has matured, the structure can be disrupted, liberating bacterial cells (Taraszkiewicz et al., 2012). The liberated cells can be transferred onto new locations or surfaces, causing an expansion of the infection.

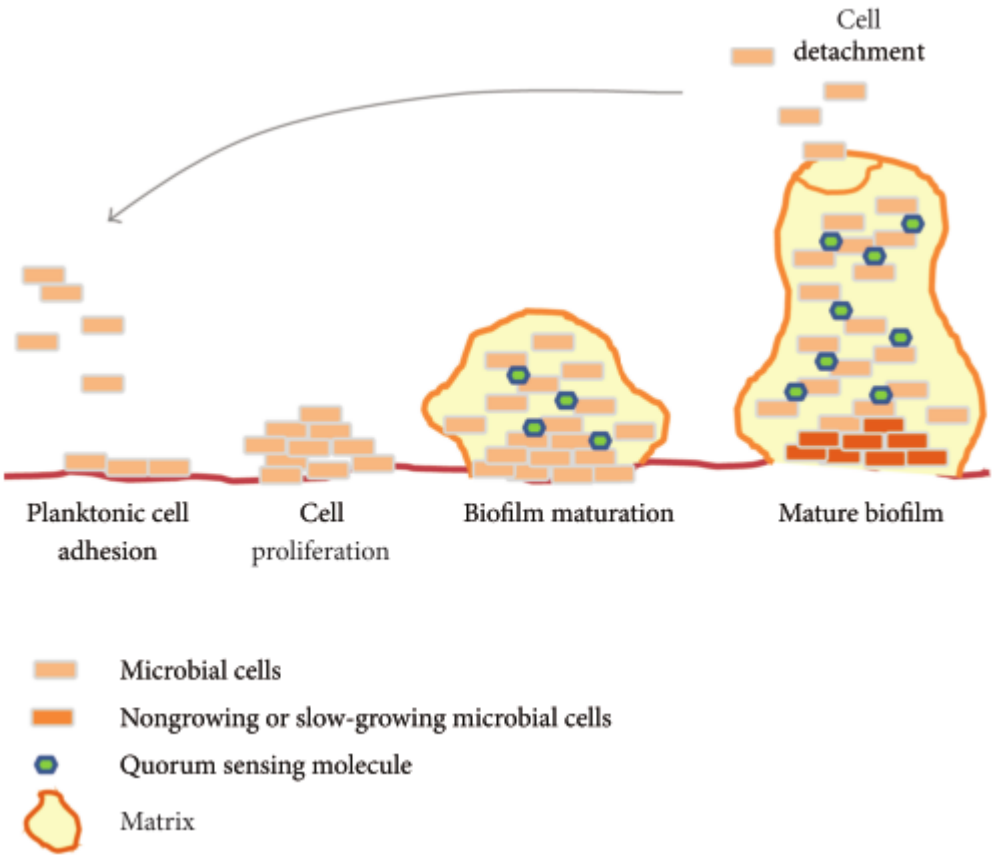

Figure 5: Biofilm formation and maturation (Taraszkiewicz et al., 2012).

A biofilm is a complex structure that provides an optimal environment for the survival of bacterial cells (Demidova-Rice et al., 2012). In addition, the biofilm has some advantages when it comes to viability and survival compared to bacteria in their planktonic state. The main advantages are increased resistance to the hosts immune response, antimicrobial agents and environmental stress, increased metabolic efficiency and increased ability to cause infections

and disease due to easier gene transfer (Thomson, 2011). There are three general mechanisms describing biofilm-resistance to antimicrobial agents, namely (a) slow or incomplete penetration through the biofilm matrix, (b) gene transfer between bacteria, and (c) development of "persister" cell populations (Hall et al., 2014).

Slow or incomplete penetration through the biofilm matrix: the extracellular polymeric substances (EPSs) matrix blocks the penetration of antimicrobial agents by several mechanisms. First, the hydrophobic EPSs matrix has a negative surface charge, preventing polar and charged molecules from reaching the inner regions of the biofilm community. Second, the EPSs matrix has pores small enough to block molecules above a certain size. Third, the EPSs matrix also have enzymes that modifies the antimicrobial agents, resulting in an inactivation/reduction of their antimicrobial activities (Pelgrift and Friedman, 2013; Hall et al., 2014).

Gene transfer between bacteria: a biofilm can increase the opportunity for gene transfer between bacteria. Bacteria resistant to antimicrobial agents can transfer the resistance gene to neighboring bacteria that are receptive (Hall et al., 2014).

Development of "persister" cell populations: development of bacterial subpopulations that are dormant and metabolically less active reduces the efficacy of antimicrobial agents. "Persister" cell populations are often non-dividing and multi-drug-resistant. In addition, they are genetically identical to the other bacterial pathogens except from an expression of antitoxins that blocks the different binding sites for antimicrobial drugs (Hall et al., 2014).

Biofilm-forming bacteria includes the Gram-negative *P. aeruginosa* and the Gram-positive *S. epidermidis* and *S. aureus* (O'Toole et al., 2000; Christensen and Brüggemann, 2014; Macià et al., 2014). *S. epidermidis* is, as mentioned earlier, a part of the human skin microbiota, but when it breaches the skin barrier and enters the bloodstream, it acts as an opportunistic pathogen (Christensen and Brüggemann, 2014).

2.2.2.2. Gram-positive and Gram-negative bacteria

Bacteria are classified as either (a) Gram-positive, or (b) Gram-negative, respectively (Jori et al., 2006; Fu et al., 2013).

Gram-positive bacteria: the outer cell wall is 15-80 nm thick, and contains up to 100 layers of peptidoglycan (**Figure 6**). The peptidoglycan layers are associated with neutral charged lipoteichoic acids and negatively charged teichuronic acids, giving the outer cell wall a net negative charge. The cell wall has a high degree of porosity due to easy diffusion of macromolecules such as glycopeptides and polysaccharides with molecular weights in the range of 30 000-60 000 Da. The outer cell wall of Gram-positive bacteria do not represent an effective permeability barrier (Jori et al., 2006; Fu et al., 2013).

Gram-negative bacteria: the peptidoglycan layer of 3 nm thickness is covered by an outer bilamellar membrane (**Figure 6**). This membrane is a 10-15 nm thick structural element composed of proteins with porin function, lipopolysaccharide trimers and lipoproteins. The heterogeneous composition gives the outer cell wall a packed negative charge, and only relatively small and hydrophilic molecules with molecular weight lower than 600-700 Da can permeate the outer cell wall due to diffusion through the porin channels (Jori et al., 2006; Fu et al., 2013).

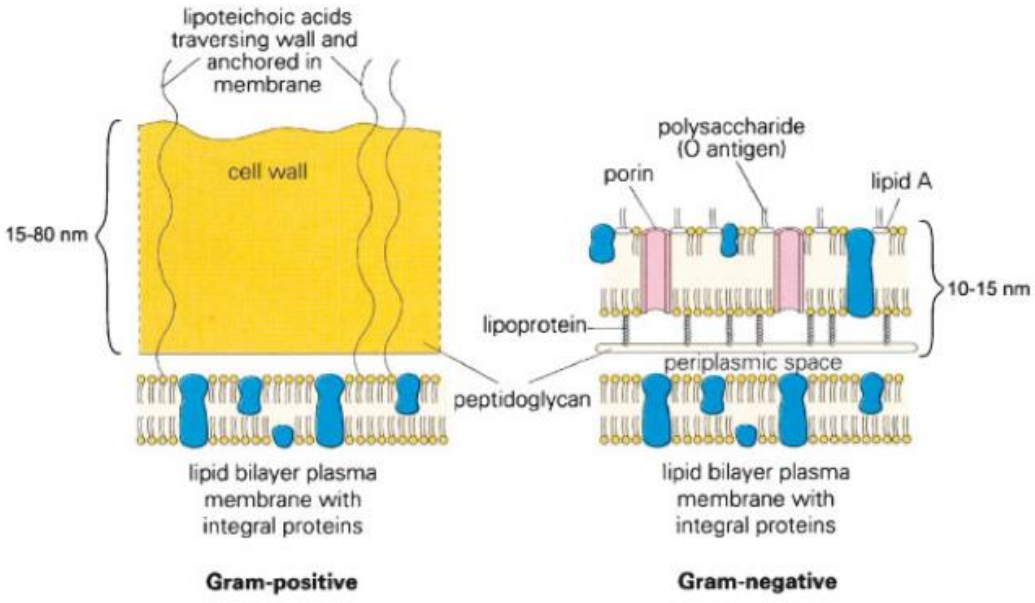

Figure 6: The structural differences of the outer cell wall between Gram-positive and Gram-negative bacteria (Jori et al., 2006).

Due to these structural differences of the outer bacterial cell wall, the permeation and penetration of e.g. antimicrobial agents is different between the Gram-positive and the Gram-negative bacteria, resulting in varying antimicrobial efficiency (Fu et al., 2013). In general, neutral, cationic and anionic molecules can permeate and penetrate the cell wall of Gram-positive bacteria while cationic molecules can permeate and penetrate the cell wall of Gram-negative bacteria, respectively (Dai et al., 2009; Fu et al., 2013).

2.2.2.3. Antibacterial treatment

Amongst many species of pathogenic bacteria, there is a rapid emerge of resistance against todays well-known and well-used antibiotics due to bacterial gene mutations and increased viability and resistivity associated with biofilm-formation (Dai et al., 2009; Percival et al., 2012). This rapid emerge in antibiotic resistance has forced human population to find new options for antibacterial treatment to which bacteria will not as easily resist. PDT is one of these optional treatments, representing a viable alternative where the mode of action is different from that of most antibiotic drugs (Jori et al., 2006). There are several favorable features of antimicrobial PDT such as broad-spectrum of action, equal killing effectiveness regardless of antibiotic resistance, and a lack of induction of PDT resistance (Jori et al., 2006; Dai et al., 2009).

2.3. Photodynamic therapy

Photodynamic therapy (PDT) has become a treatment option when it comes to treating various diseases such as infections, actinic keratosis (AK), aged-related macular degeneration and cancer (e.g. oesophagus, bladder, skin). The treatment involves a combination of a molecule called photosensitizer (PS) and visible light of an appropriate wavelength matching the absorption spectrum of the PS in addition to oxygen (O_2) (Bechet et al., 2008; Tan et al., 2013). Individually, these three components are harmless but when combined, they form either reactive oxygen species (ROS) or singlet oxygen ($^1O_2$), leading to apoptotic and necrotic cell death (Dai et al., 2012; Tanaka et al., 2012). After this initial photo damage, PDT results in a complex cascade of cell eradication involving photochemical, immunological and physiological reactions (Fotinos et al., 2006).

2.3.1. Photon absorption

After photon absorption, the PS converts to an excited state, which further reacts with oxygen. When excited PS reacts with O_2, the process goes one of the two ways, depending on the type of reaction (Taraszkiewicz et al., 2012).

Type I reaction involves transfer of electrons from the excited PS to a substrate, e.g. unsaturated phospholipids in the membrane or aminolipids (**Figure 7**). This electron transfer leads to the production of lipid-derived radicals or water-derived hydroxyl radicals (HO·) that further can react with other biomolecules and oxygen to yield hydrogen peroxide (H_2O_2). H_2O_2 can cause lipid peroxidation or lead to ROS production, causing damaging action to cellular structures such as the cell membrane, mitochondria, lysosomes and nuclei (Fotinos et al., 2006; Taraszkiewicz et al., 2012).

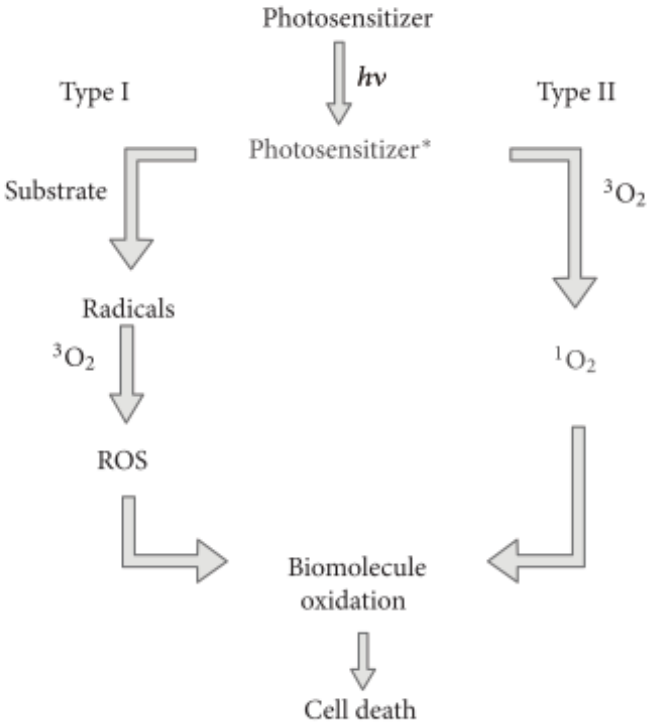

Figure 7: Scheme of the photodynamic process. The excited photosensitizer goes one of two ways, type I reaction or type II reaction, both resulting in biomolecule oxidation and cell death (Taraszkiewicz et al., 2012).

Type II reaction involves transfer of energy from the excited PS to ground-state molecular oxygen (O_2), leading to a formation of excited oxygen ($^1O_2$) (**Figure 7**). $^1O_2$ is a very reactive molecule that can oxidize biomolecules found in the cell such as proteins, nucleic acid and lipids. Biomolecule oxidization leads to cell damage and death (Taraszkiewicz et al., 2012).

2.3.2. The photodynamic therapy agent

Since the PS has to be in an excited state to be able to react with oxygen or other substrates, the photodynamic therapy agent (PDTA) has to be light-sensitive and absorb light, e.g. dyes like methylene blue, phtalocyanine and toluidine blue (**Figure 8**). The PDTA can also be a precursor, or a prodrug, to a light sensitive molecule, e.g. the naturally occurring haem precursor 5-aminolevulinic acid (5-ALA) and its derivatives (Fotinos et al., 2006; Li et al., 2013).

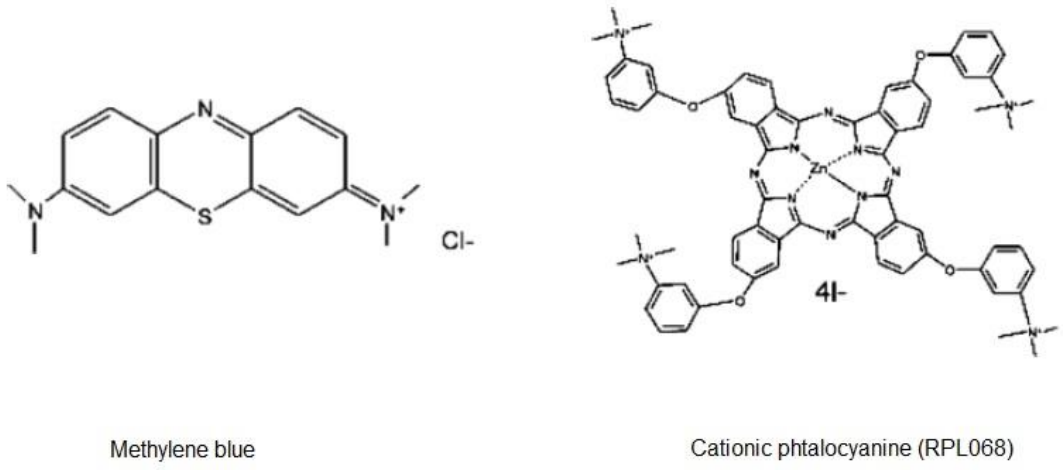

Figure 8: Chemical structure of methylene blue (left) and cationic phtalocyanine (right) (Sharma et al., 2012).

2.3.2.1. 5-aminolevulinic acid and protoporphyrin IX

5-ALA is a naturally occurring amino acid and precursor to the photoactive compound protoporphyrin IX (PpIX) in the biosynthesis of haem (Fotinos et al., 2006). The haem biosynthesis takes place in the cytosol and mitochondria. 5-ALA is an endogenous substance formed by a conversion of glycine and succinyl coenzyme A catalyzed by the enzyme 5-aminolevulinate synthase (ALAS). Endogenous formation of 5-ALA is inhibited by haem through a negative feedback control mechanism. The formation of 5-ALA takes place in the mitochondria before it reaches the cytosol. In the cytosol, 5-ALA undergoes different

conversions catalyzed by several enzymatic reactions, resulting in a molecule called protoporphyrinogen (PROTO) III in the mitochondria. PROTO III undergoes a decarboxylation, leading to the formation of PpIX. When the enzyme ferrochelatase inserts a ferrous iron into PpIX, haem is produced. Ferrochelatase is a rate-limited enzyme, leading to an accumulation of PpIX in the presence of exogenous 5-ALA (Wachowska et al., 2011). Exogenous 5-ALA also bypasses the haem inhibition mechanism (Kennedy and Pottier, 1992).

In e.g. open wounds, inflammation, psoriasis and chronic sun damage, accumulation of PpIX occurs especially in the damaged cells due to easy permeation of 5-ALA into the epidermis as compared to healthy/normal epidermis (Kennedy and Pottier, 1992; Fotinos et al., 2006; Menezes et al., 2014). Factors affecting the permeation can be the metabolic, environmental and morphological differences. In addition, the biosynthetic pathway of haem differs between malignant and non-malignant cells, leading to an increased PpIX accumulation due to decreased ferrochelatase enzyme activity and limited availability of iron in e.g. tumor cells (Wachowska et al., 2011).

PpIX (**Figure 9**) is an immediate precursor to haem in addition to be the photosensitizing agent in 5-ALA-mediated PDT (Menezes et al., 2014). PpIX has excitation wavelengths (λ_{ex}) of 646, 630 and 546 nm, giving an average singlet oxygen yield of approximately 56 % (Redmond and Gamlin, 1999).

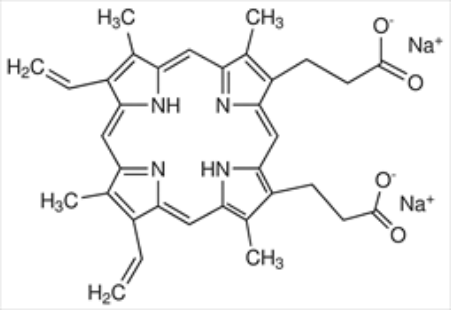

Figure 9: Chemical structure of protoporphyrin IX disodium (Martindale, 2014).

5-ALA has an amine terminal and a carboxylic terminal that allows the molecule to be present as a charged zwitterion under physiological conditions (**Figure 10**). Due to this property, 5-ALA has limited capacity to reach and enter a target cell under biological circumstances, leading to a low oral bioavailability and photodynamically efficient dose of PpIX (Fotinos et al., 2006). The low oral bioavailability is also a result of hepatic first pass metabolism and formation of PpIX in gastrointestinal mucosal cells (Wachowska et al., 2011).

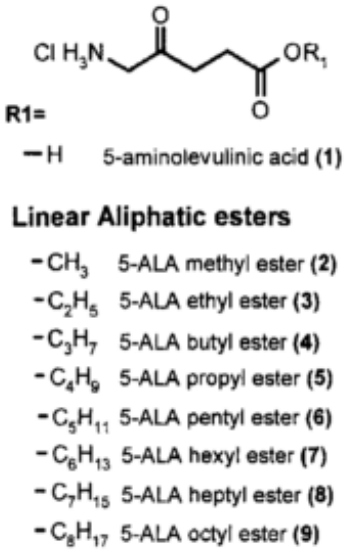

Figure 10: Chemical structure of 5-aminolevulinic acid (1) including some of the derivatives such as methylaminolevulinate (2) and hexylaminolevulinate (7) (Fotinos et al., 2006).

The use of 5-ALA have several limitations. The 5-ALA molecule is hydrophilic, showing poor penetration through cell membranes, biological barriers and skin, leading to a production and accumulation of endogenous PpIX. For skin, this PpIX accumulation will be restricted to a superficial skin surface of 2-3 mm (Fotinos et al., 2006; Wachowska et al., 2011). This limitation can be improved by increasing the lipophilicity of 5-ALA through molecule alterations, resulting in lipophilic 5-ALA derivatives. On todays marked, there are two 5-ALA derivatives that have gained marketing authorization; hexaminolevulinate (HAL; Hexvix®) (**Figure 10**), for the detection and management on non-muscle invasive bladder cancer (NMIBC), and methylaminolevulinate (MAL; Metvix®) (**Figure 10**), for the treatment of AK and superficial basal cell carcinoma (BCC). There is also a 5-ALA preparation on the marked for the topical treatment of AK called Levulan® Kerastick® (DUSA Pharmaceuticals, 2014).

PDT using topical application of 5-ALA is a selective and safe treatment due to low permeation of 5-ALA in normal skin tissue (Kennedy and Pottier, 1992). After topical application, 5-ALA penetrates the *stratum corneum* before it diffuses through the epidermis and in to the dermis. Scarring of the skin is minimalized with PDT due to low development of PpIX by the dermal cells.

2.3.3. Antimicrobial PDT

Most bacteria produce porphyrins from the precursor 5-ALA through the haem biosynthetic pathway (Hamblin and Hasan, 2004), as described for mammalian cells. The bacterial pathway is not similar to that found in mammalian cells due to the lack of mitochondria, giving a poor understanding of the haem biosynthesis (Frankenberg et al., 2003).

The susceptibility of PDT differs between Gram-positive and Gram-negative bacteria due to differences in the outer cell membrane (**Figure 11**) (Hamblin and Hasan, 2004; Sharma et al., 2012; Taraszkiewicz et al., 2012). Gram-positive bacteria are more susceptible to PS molecules that are neutral, anionic and cationic. Gram-negative bacteria are more susceptible to cationic PS molecules due to the strong and negatively charged permeability barrier.

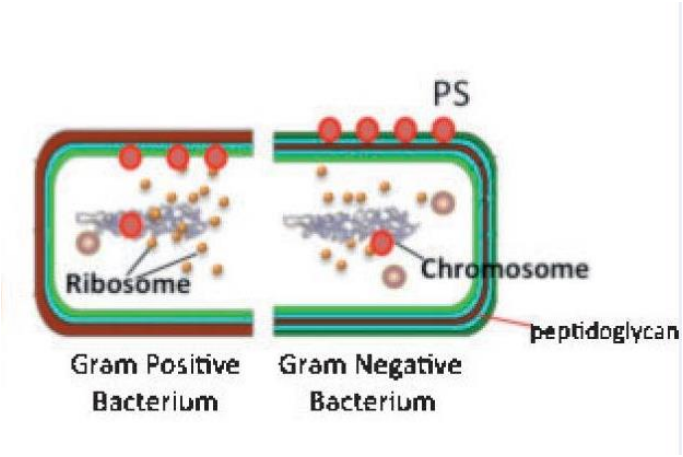

Figure 11: Penetration of PS through the bacterial cell wall. In Gram-positive bacteria, the PS can penetrate through the cell wall and plasma membrane, reaching the cytosol. In Gram-negative bacteria, the PS has difficulties reaching the cytosol due to the strong permeability barrier of the outer cell wall (Sharma et al., 2012).

Two different mechanisms have been proposed for the lethal damage to bacteria by PDT, namely (a) DNA damage, and (b) damage to the cytoplasmic membrane (Hamblin and Hasan, 2004; Taraszkiewicz et al., 2012).

DNA damage involves breaks in single-stranded and double-stranded DNA. The mechanism of DNA damage may not be the main cause of bacterial cell death due to protection of the cell that involves DNA repair mechanisms (Hamblin and Hasan, 2004; Taraszkiewicz et al., 2012).

Damage to the cytoplasmic membrane involves disruption of proteins involved in transport and membrane structure. This disruption leads to a leakage of cellular constituents and inactivation of membrane transport systems and enzymes (Hamblin and Hasan, 2004; Taraszkiewicz et al., 2012).

The physiological state of the bacteria is important for the efficacy of antimicrobial PDT (APDT). The cells in the logarithmic phase of growth is more susceptible to PDT than the cells in the stationary phase (Jori et al., 2006).

2.3.3.1. In-vitro and in-vivo studies of antimicrobial PDT

There are several studies showing the effectiveness of APDT.

Simonetti et al. (2011) investigated the efficacy of a single treatment of APDT with RLP068/Cl (a tetracationic Zn(II) phtalocyanin) against a strain of methicillin-resistant *S. aureus* (MRSA). The study was an in-vivo experiment, using a mouse model of a surgical wound infection induced with MRSA. The light source was a diode laser at 689 nm with a light dose of 60 J/cm^2. The results showed, after two days, a significantly lower bacterial count in infected animals after APDT with 0.3 % RLP068/Cl ($3.3x10^6 \pm 4.0x10^6$ CFU/ml) compared to infected control group ($1.0x10^9 \pm 9.6x10^8$ CFU/ml) and APDT placebo group ($8.5x10^8 \pm 7.0x10^8$ CFU/ml).

Hashimoto et al. (2012) tested, both in-vitro and in-vivo, the APDT effect with HB:La^{3+} (Hypocrellin B with lanthanide ions) against multidrug-resistant *P. aeruginosa*. The light sources used were a light-emitting diode with blue and red light (460±20 nm and 645±10 nm, respectively). The in-vitro experiment showed an approximate log reduction of 5 for *P. aeruginosa* after 8 minutes of irradiation with a light dose of 96 J/cm^2 compared to control group (no irradiation and photosensitizer), LED groups (blue or red irradiation) and HB:La^{3+} group (only 10 µM photosensitizer) that did not show any bactericidal effect. There was no significant difference in bacterial load between blue and red LED for the experimental group (HB:La^{3+} combined with blue or red LED). The in-vivo study was performed in mice with *P. aeruginosa* infected third degree burns. No decrease in bacterial count was observed in control

group, LED groups and HB:La^{3+} group. The experimental group showed an approximate log reduction of 2 for both blue and red LED (no significant difference).

Vecchio et al. (2013) investigated the effect of APDT with RLP068/Cl against a MRSA infected scratch wound in mice. The APDT efficacy with RLP068/Cl was compared to APDT with toluidine blue O (TBO) using light sources of 690 and 635 nm, respectively. The illumination time for both photosensitizers was 14 minutes corresponding to a total dose of 84 J/cm^2. The in-vivo study showed a significant reduction of the bacterial burden in the wound using a bioluminescent strain of MRSA with a RLP068/Cl concentration of 75 µM and a light dose of 84 J/cm^2 compared to PDT with 75 µM TBO and a light dose of 84 J/cm^2. A bacterial re-growth was observed the following days after PDT with TBO. An additional in-vitro study showed a total killing of MRSA using 100 nM RLP068/Cl and a light dose of 5 J/cm^2.

Li et al. (2013) investigated the effect of APDT with aminolevulinic acid (ALA) on antibiotic-resistant staphylococcal biofilm. The biofilm-forming strains were MRSA and methicillin-resistant *S. epidermidis* (MRSE). The concentration of ALA was 40 mM, and the light source was set at 635 nm. The light doses used were 0, 100, 200 and 300 J/cm^2. The experimental groups were the following: TSB group (no ALA and no light irradiation), light group (light dose of 300 J/cm^2 and no ALA), ALA group (ALA with no PDT), ALA-PDT 1 (light dose 100 J/cm^2), ALA-PDT 2 (light dose 200 J/cm^2) and ALA-PDT 3 (light dose 300 J/cm^2). TSB group, light group and ALA group were found to be not toxic to the biofilm, showing no differences in survival of MRSA or MRSE. The results for the ALA-PDT groups showed a decrease in number and size of colony masses with an increased light dose. Few aggregated colonies were observed in both MRSA and MRSE biofilms in the presence of 40 mM ALA and a light dose of 300 J/cm^2. This can suggest an absence of classic biofilm morphology.

A Phase IIa randomized, placebo-controlled study executed by Morley et al. (2013) determined the effect of APDT against bacteria that had colonized chronic leg ulcers and chronic diabetic foot ulcers. The bacteria found after screening were *S. aureus* and coliforms. Patients with leg ulcers and diabetic foot ulcers were randomized such as for each ulcer type, 50 % of the patients received PDT treatment and light, and 50 % received placebo and light. The PS was the cationic 3,7-bis(N,N-dibutylamino) phenotiazin-5-ium bromide (PPA904) in the concentration 500 µM. The light source was a red light (570-670 nm), and the total dose was 50 J/cm^2. The results for the patients that received active treatment showed a significant post-treatment bacterial load reduction as compared to patients that received placebo.

2.3.4. Drug delivery of PDT agent

Most of the PDT agents used are hydrophobic. Due to this characteristic, the photo-physical (formation of ROS and $^1O_2$), biological and chemical (solubility) properties are affected by strong hydrophobic interactions between the molecules in the presence of an aqueous environment (Bechet et al., 2008). Encapsulation is one strategy to protect the PDTA from the aqueous environment and avoid reduced PDT efficiency due to molecule aggregation. Encapsulation of the PS can also help overcome the permeability barrier associated with Gram-negative bacteria, resulting in enhanced PDT efficacy (St Denis et al., 2011).

2.4. Nanoparticles as drug delivery system

Encapsulation of the PDT agent in colloidal preparations such as liposomes, micelles, nanoemulsions and nanoparticles (NPs) have been proposed as an effective administration of drug molecules having problems with e.g. poor water solubility, toxicity and low bioavailability. In several cases, nanosystems using polymers and lipids have shown improved drug bioavailability, modified drug pharmacokinetics and protection of the drug from enzymatic attack (Sonvico et al., 2006).

In antimicrobial PDT, there are several advantages using PDT agents encapsulated in NPs such as (a) reduced drug resistance, (b) improved treatment selectivity, and (c) nonimmunogenic matrix (Hamblin and Hasan, 2004).

Reduced drug resistance: use of NPs limits the target cell's ability to pump the drug molecule back out, resulting in reduced drug resistance (Hamblin and Hasan, 2004).

Improved treatment selectivity: use of localized delivery agents improves the treatment selectivity achieved by either active or passive targeting, depending on the charged surface of the nanoparticle (Hamblin and Hasan, 2004).

Nonimmunogenic matrix: using biodegradable and biocompatible matrices such as liposomes, poly(lactic-co-glycolic acid) (PLGA) and cyclodextrins makes the NPs nonimmunogenic (Hamblin and Hasan, 2004).

NPs made of polysaccharides and lipids are considered safe because of the biodegradable and biocompatible properties of the materials (Sonvico et al., 2006).

2.4.1. Lecithin

Lecithin is a mixture of natural phospholipids found in e.g. soybeans and egg yolk (Budai et al., 2013), and due to variations in origin and phospholipid content, the physicochemical properties may vary. The phospholipids differ in a) composition, e.g. length of fatty acid chains, and b) polarity of the head groups. The most common phospholipids are phosphatidylcholine (**Figure 12**) and phosphatidylethanolamine (Hafner et al., 2011). Lecithin is considered to be a safe and biocompatible excipient, and has frequently been used in the preparations of various delivery systems such as micelles, liposomes, micro- and nanoemulsions and solid lipid nanoparticles (Sonvico et al., 2006; Senyiğit et al., 2010; Tan et al., 2011; Hafner et al., 2011; Özcan et al., 2013).

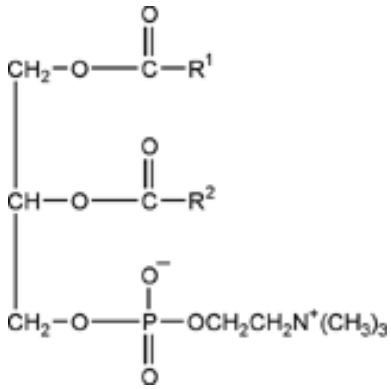

Figure 12: Chemical structure of phosphatidylcholine where R^1 and R^2 are fatty acids that can be different/identical (Pharmaceutical Excipients, 2014a).

2.4.2. Chitosan

2.4.2.1. Structure of chitosan

Chitosan is a cationic polysaccharide consisting of the copolymers glucosamine and N-acetyl-glucosamine linked by β-1,4-glycosidic bonds (**Figure 13**). Chitosan is a derivative of chitin, a natural biopolymer found in e.g. mushrooms, crustaceans and the exoskeleton of insects (Dai et al., 2011). The characteristics of chitosan are influenced by its molecular weight (MW) and degree of deacetylation (DD) (Berger et al., 2004), representing the proportion of deacetylated units of the amine functional groups compared to chitin.

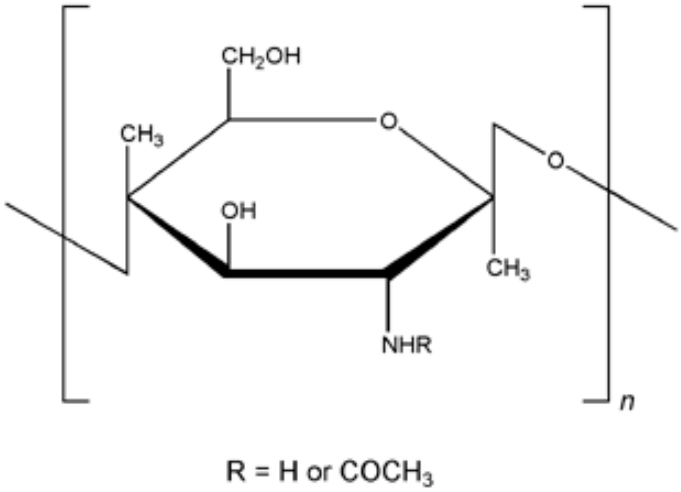

Figure 13: Chemical structure of chitosan where R = glucosamine (H) or N-acetyl-glucosamine ($COCH_3$) and n = number of sugar units (Pharmaceutical Excipients, 2014b).

Chitosan is subdivided into three different types based on the molecular weight (Wong, 2009), namely low molecular weight chitosan with a MW < 150 kDA, medium molecular weight chitosan and high molecular weight chitosan with a MW = 700-1000 kDA. Chitosan is a weak base with a pKa value of 6.2-7. Due to this, chitosan is easily soluble in aqueous acidic solutions and slightly soluble at pH 7.4 and higher. Further, the solubility of chitosan in acidic media is depending on the degree of deacetylation (Wong, 2009).

2.4.2.2. The biopharmaceutical properties of chitosan

Chitosan is an interesting polysaccharide in drug delivery, and in general, due to its biopharmaceutical properties such as biocompatibility, biodegradability, bio-adhesion and enhanced penetration across barriers (e.g. skin) (Senyiğit et al., 2010).

The biocompatibility of chitosan is related to its non-toxicity, in addition to not causing irritation and allergic effects. In the US, chitosan is designated as GRAS (Generally Recognized As Safe) when it comes to the use of chitosan in the food industry (Baldrick, 2010). In Finland, Italy and Japan, chitosan is listed as a food additive. Further, chitosan has also been used as a dietary supplement. Several reports have shown that dietary levels of chitosan up to 5 % in rats and mice were well tolerated and showing no toxicity; the oral LD_{50} value was found to be over 16 g/kg body weight of mouse (Wong, 2009; Baldrick, 2010).

Bio-adhesion of chitosan to e.g. mucus is due to an electrostatic interaction between the positively charged chitosan and the negatively charged mucus gel layer. Enhanced transmucosal drug absorption is one effect to be seen after bio-adhesion of chitosan to mucosa (Wong, 2009).

The in vivo degradation of chitosan is performed by lysozymes through depolymerization, producing N-acetyl-glucosamine; the degree of degradation is dependent on the DD (Wong, 2009; Baldrick, 2010).

2.4.2.3. Chitosan and antimicrobial action

The characteristics of chitosan give rise to different mechanisms of action against microbes such as (a) association of chitosan with negatively charged cell walls and plasma membranes, (b) binding to DNA, (c) chelating of metals, and (d) faster wound healing. Since chitosan has multiple antimicrobial actions, there is unlikely that the microbes will undergo multiple mutations to achieve resistance (Pelgrift and Friedman, 2013).

Association of chitosan with negatively charged cell walls and plasma membranes: at pH lower than the pKa, the amino functional groups will be protonated and the chitosan will get an overall positive charge. By associating the positively charged chitosan with negatively charged cell walls and plasma membranes of microbial cells, chitosan will have an antimicrobial effect caused by enhanced membrane permeability, osmotic damage and subsequent leakage of cytoplasmic constituents (including ions and proteins). High molecular weight chitosan will have greater antimicrobial effect against Gram-positive bacteria while low molecular weight chitosan will have greater antimicrobial effect against Gram-negative bacteria (Kishen et al., 2008; Pelgrift and Friedman, 2013; Shrestha et al., 2014).

Binding to DNA: the positively charged chitosan can also bind to negatively charged DNA in microbes. The antimicrobial effect is seen due to inhibition of mRNA transcription and the following protein translation (Pelgrift and Friedman, 2013).

Chelating of metals: chitosan can decrease the activity of metalloproteins (e.g. enzymes, storage proteins, transcription factors) by specific interactions with metals (i.e. iron, copper, zinc and manganese). With reduced availability of essential metals, microbes will not be able to cause disease since metals are an important requirement during processes in pathogenesis ranging from bacterial metabolism to virulence factor expression (Wong, 2009; Pelgrift and Friedman, 2013; Porcheron et al., 2013).

Faster wound healing: by inhibiting the release of inflammatory cytokines, chitosan can cause a faster healing of the wound and decreased probability of wound infection. In addition, chitosan has shown to have a role in the haemostatic action, activation of macrophages and stimulation of cell proliferation and histoarchitectural tissue organization (Baldrick, 2010; Pelgrift and Friedman, 2013).

2.4.3. Nanoparticles made of lipids and polysaccharides

The formation of lecithin/chitosan (LC) nanoparticles (NPs) is a result of a supra-molecular self-organizing interaction between the positively charged polysaccharide and the negatively charged lipid material, without preliminary vesicle formation (Sonvico et al., 2006; Hafner et al., 2011). Lecithin and chitosan are favorable constituents due to their biocompatibility in addition to chitosan's biocompatible, bio-adhesive and antimicrobial properties (as described above) (Hafner et al., 2011). There are several articles showing that LCNPs are suitable carriers for hydrophobic drugs such as progesterone (Sonvico et al., 2006), quercetin (Tan et al., 2011), melatonin (Mrhar et al., 2009; Hafner et al., 2011), natamycin (Bhatta et al., 2012), hydrochlorotiazide (Chadha et al., 2012), tamoxifen (Barbieri et al., 2013) and topical steroids (Senyiğit et al., 2010; Özcan et al., 2013; Özcan et al., 2013). In addition, the majority of the articles report of LCNPs mucoadhesive properties.

Tan et al. (2011) showed, both in-vitro and in-vivo, that quercetin-loaded NPs could enhance the permeation of quercetin in skin within 12 hours of application compared to a quercetin propylene glycol solution. In addition, the NPs could also have the possibility to promote the accumulation of quercetin in the epidermis.

Özcan et al. (2013) showed that there was an improved accumulation of diflucortolone valerate (DFV) in the *stratum corneum* and epidermis using DFV-loaded NPs and DFV-loaded NPs in a chitosan gel formulation compared to a DFV commercial cream formulation, respectively. Both ex-vivo permeation and in-vivo studies were performed. Moreover, the experiment also showed a sustained release of DFV up to 24 hours with lecithin/chitosan nanoparticle formulation.

In another study, Özcan and his research group compared the accumulation of betamethasone valerate (BMV) using LCNPs, PLGA NPs and a BMV commercial cream in addition to LC and PLGA NPs in chitosan gel formulation. The ex-vivo permeation study showed that LCNPs had higher accumulation of BMV in epidermis compared to PLGA NPs (Özcan et al., 2013). In

addition, use of LC and PLGA NPs in chitosan gel showed higher retention of BMV compared to commercial cream, even though the concentration of BMV was ten times higher in the commercial cream.

A study done by Bhatta et al. (2012) showed that natamycin-loaded LCNPs exhibited a higher retention time compared to the commercial natamycin suspension Natamet® regarding in-vivo precorneal retention.

In two studies, Mrhar et al. (2009) and Hafner et al. (2011) showed, in-vitro, that melatonin-loaded LCNPs using S45 lecithin enhanced the permeability of melatonin through both Caco-2 cell monolayer and porcine ear skin compared to an aqueous melatonin solution.

Senyiğit et al. (2010) showed that the use of LCNPs loaded with clobetasol-17-propionate (CP) had the opportunity to enhance the accumulation of CP in pigskin compared to chitosan gel and commercial cream. The results also showed a non-significant permeation of CP through the skin.

The results presented above suggest that the use of lecithin/chitosan NPs as drug carriers provides a great potential for improvement of both drug accumulation and permeation across different biological barriers.

2.5. New Chemical Entity

Photocure ASA provides all the information about this new chemical entity (NCE).

NCE is a derivative of the naturally occurring amino acid 5-ALA. Cell uptake of NCE leads to an intracellular accumulation of the endogen PS PpIX, as described earlier.

NCE is soluble in water (3.6 g/g water), and the free amino group in the molecule has a pKa of approximately 8.3. The stability in aqueous environments is poor, resulting in a degradation of NCE through hydrolysis.

3. Aims of the study

The main aim of this study was to evaluate the efficacy and potential of a New Chemical Entity (NCE) in combination with photodynamic therapy (PDT) against biofilm-forming *Staphylococcus epidermidis*. Due to rapid degradation and poor stability in aqueous environments, NCE was entrapped in nanoparticles made of lecithin and chitosan. The use of nanoparticles with an overall positive surface charge provides an opportunity to enhance the bacterial/biofilm permeability, making the bacterial cell membrane/biofilm matrix more susceptible for NCE. Prior to the evaluation of efficacy and potential, a biofilm elimination method needed to be optimized.

The specific aims, described in more detail, were:

- Development of nanoparticles containing NCE in a sufficient concentration for further use in evaluation of biofilm elimination
- Optimization of a biofilm elimination method to be used in evaluation of NCE-mediated PDT against *S. epidermidis* biofilm
- Anti-biofilm evaluation of free NCE in combination with light exposure
- Anti-biofilm evaluation of nanoparticles containing NCE in combination with light exposure
- Anti-biofilm evaluation of free NCE and nanoparticles containing NCE without exposure to light

4. Materials and Methods

4.1.1. Materials

Acetic acid (≥ 99.8 %), Sigma-Aldrich, St. Louis, USA

Acetonitrile, CHROMASOLV® gradient grade for HPLC, Sigma-Aldrich, St. Louis, USA

Ammonium acetate, VWR International, Leuven, Belgium

Buffer solutions, pH 4 and 7, AVS Titrinorm®, VWR BDH PROLABO, Leuven, Belgium

Chitopharm™ M, Chitinor AS, Haugesund, Norway

Crystal violet, Merck KGaA, Darmstadt, Germany

D(+)glucose anhydrous, Merck KGaA, Darmstadt, Germany

Distilled water

Ethanol, p.a., Sigma-Aldrich, St. Louis, USA

Filtered water, MILLI-Q BIOCELL, 0.22 µm, Bergman AS, Trondheim, Norway

Lipoid S 100 (soybean lecithin with > 94 % (w/w) phosphatidylcholine), Lipoid GMBH, Ludwigshafen, Germany

Methanol, CHROMASOLV® for HPLC, Sigma-Aldrich, St. Louis, USA

New Chemical Entity, Photocure ASA, Oslo, Norway

Potassium chloride, Merck KGaA, Darmstadt, Germany

Potassium phosphate monobasic (purity ≥ 99.0 %), Sigma-Aldrich, St. Louis, USA

Sodium chloride (purity ≥ 99.5 %), Fluka Analytical, Sigma-Aldrich, St. Louis, USA

Sodium hydroxide (purity ≥ 98 %), Sigma-Aldrich, St. Louis, USA

Sodium phosphate dibasic (purity ≥ 98.5 %), Sigma-Aldrich, St. Louis, USA

Tryptic soy agar (Microbiologically tested), Sigma-Aldrich, St. Louis, USA

Tryptic soy broth, Sigma-Aldrich, St. Louis, USA

Vancomycin hydrochloride from *Streptomyces orientalis*, Sigma-Aldrich, St. Louis, USA

4.1.2. Bacterial strain

Staphylococcus epidermidis ATCC 35984 (RP62A 42-77), CCUG: Culture Collection, University of Göteborg, Sweden

4.1.3. Instruments, utensils and equipment

Accu-jet® pro Pipette Controller, Brand, Wertheim, Germany

Acrodisc® 32 mm Syringe Filter with 5 µm Supor® Membrane, Sterile, Non-pyrogenic, Pall International, Fribourg, Switzerland

Acrodisc® 25 mm Syringe Filter with 0.2 µm Supor® Membrane, Sterile, Non-pyrogenic, Pall International, Fribourg, Switzerland

Analytical scale, Sartorius BP211D, KEBO Labs AS, Norway

BD Falcon, Serological pipettes 5 ml, Sterile, Non-pyrogenic, Becton Dickinson Labware, New Jersey, USA

BD Falcon, Serological pipettes 10 ml, Sterile, Non-pyrogenic, Becton Dickinson Labware, New Jersey, USA

BD Plastipak™, 1 ml syringes, Becton, Dickinson and Company, New Jersey, USA

BD Plastipak™, 20 ml Luer syringes, Becton, Dickinson and Company, New Jersey, USA

Centrifuge tubes with conical bottom, high performance, 15 ml, sterile,VWR International, Leuven, Belgium

Centrifuge tubes with conical bottom high performance, 50 ml, sterile, VWR International, Leuven, Belgium

Color Squid, magnetic stirrer, IKA, Staufen, Germany

Disposable microcentrifuge tubes w/lid, 1.5 ml, sterile, Brand GMBH, Wertheim, Germany

Beckman L8-M Ultracentrifuge, Beckman Instruments Inc., Palo Alto, USA; with SW60Ti ROTOR, Beckman Coulter Inc., California, USA

Biocap LAF bench, 230 V, 50 Hz, 73 W, Erlab, Cedex, France

Biofuge Pico Heraeus table centrifuge, Thermo Electronic Corporations, Osterode, Germany

CertoClav Multicontrol autoclave, CertoClav GMBH, Traun, Austria

DEN-1 McFarland Densitometer, Biosan, Riga, Latvia

Infors HT multitron shaker, Infors AG, Bottmingen/Basel, Switzerland

NICOMP Submicron particle sizer, Model 370, Nicomp Particle sizing systems, Santa Barbara, USA; with Disposable culture tubes, Borosilicate glass, 6x50 mm, Kimble Chase, USA

Metrohm 744 pH Meter, Metrohm AG, Herisau, Switzerland

Polypropylene Round-Bottom Tubes, 14 ml, Sterile, Non-pyrogenic, BD Falcon: Becton, Dickinson and Company, New Jersey, USA

QIAfilter™ Mega-Giga Cartridge, Qiagen GmbH, Hilden, Germany

TC Microwell 96 F w/lid Nunclon D Si (nunclon delta surface), Thermo Fisher Scentific Nunc A/S, Roskilde, Denmark

Termaks Laboratory Incubator Series 8000, Termaks, Bergen, Norway

Ultrasonic Processor 500 W, Sigma-Aldrich, St. Louis, USA

Universal indicator, pH 1-14, Merck, Darmstadt, Germany

VersaMax ELISA Microplate Reader, Molecular Devices, Sunnyvale, USA

Vertical laboratory autoclave, Getinge AB, Gothenburg, Sweden

Waters e2795 Separation module, Waters 2489 UV/Visible Detector, Waters, Milford, USA; with ZIC®-HILIC 3.5 µm, 200 Å (150x4.6 mm) and ZIC®-HILIC Guard Column (20x2.1 mm) from Merck kGaA, Darmstadt, Germany

Zetasizer Nanoseries, Model ZEN 2600, Malvern Instruments Limited, Malvern, UK

4.1.4. Computer programs

High Performance Liquid Chromatography: Empower3 Chromatography Software

Photon Correlation Spectroscopy: CW 388 version 1.68

Zeta potential: Zetasizer Software 7.03

ELISA reader: SoftMax Pro Software version 5.4.1

4.2. Characterization of nanoparticles

4.2.1. Preparation of lecithin/chitosan nanoparticle suspension containing NCE

Lecithin/chitosan nanoparticles (LCNPs) were prepared by injecting an alcoholic lecithin solution into an aqueous chitosan solution by a modified method of Sonvico et al. (2006). As a first step, an ethanolic solution of lecithin 10 % (w/v) containing 2.5 % (w/v) NCE was prepared. The nanoparticles were obtained by slowly adding 4 ml of the ethanolic lecithin solution through a glass pipette (injection rate 4 ml/min) under mechanical stirring into 46 ml of a 0.04 % (w/v) chitosan solution. The chitosan solution was prepared by diluting with distilled water 1 % (w/v) chitosan solution in 0.5 % acetic acid. In the final suspension, lecithin/chitosan ratio was 20:1 (w/w) and the content of NCE was 0.2 % (w/v). Empty nanoparticles, serving as a control, were prepared under the same conditions.

4.2.2. Determination of entrapment efficiency

The entrapment efficiency (EE) was determined using ultracentrifugation as a separation method, followed by high performance liquid chromatography (HPLC) analysis. A known amount of nanoparticle suspension was centrifuged at 10.0 °C and 167000 x g for 2 hours. The pellets were then dissolved in 1 ml of methanol prior to the HPLC analysis. The content of NCE was determined in both the supernatants and pellets.

4.2.3. HPLC analysis

The HPLC method used was based on a document provided by a Norwegian GMP certified chemical analysis contract lab, Vitas AS (Oslo Innovation Center). The two mobile phases, A and B (1 and 1.1 L, respectively), consisted of acetonitrile and filtered water (MILLI-Q) 1:10

and 2:11 (v/v), respectively, in addition to 1.5 g ammonium acetate for each mobile phase. A dilution solvent (DS) was made by blending the mobile phases A and B 2:10 (v/v). To obtain a standard curve in DS, a NCE stock solution was prepared in a concentration of 5 mg/ml. The six standard solutions of 0.05, 0.1, 0.5, 1, 2 and 4 mg/ml of NCE were made by diluting the stock solution with appropriate volumes of DS. The standard solutions were freshly prepared prior to the analysis. The flow rate was set to 1.0 ml/min, and monitored with a UV/Visible detector set at 270 nm. The run time was 12 minutes and the injection volume was 20 µl. The temperature of the column and the samples during the separation process was set at 40 and 8 °C, respectively. The gradient program for the mobile phases were set to 90 % B at initial time, reduced to 0 % B at 7 minutes, and then increased to 90 % B at 11 minutes. All analysis were performed in triplicates, and the acquisition and processing of data were performed with a DELL computer using Empower3 Chromatography Software.

4.2.4. Particle size analysis

The particle size distribution was determined using photon correlation spectroscopy (PCS), also known as dynamic light scattering (DLS), and the determination was performed on the NICOMP Submicron particle sizer model 370. Before the actual measurement, the test samples were prepared in a clean area with sterile/particle free equipment to avoid contamination with particles from the environment. Preparation and handling were done in a laminar airflow bench (LAF bench). Test tubes were filled with distilled water and sonicated for 15 minutes in an ultrasonic bath. Before use, test tubes were rinsed with filtered water (0.2 µm pore sized syringe filter). Samples were diluted with filtered water to obtain intensity in the range 250-350 KHz. The number of runs set for each sample was set to 3 cycles with 10 minute cycle duration.

4.2.5. Zeta potential

Zeta potential (ZP) was measured using Zetasizer Nano Z 2600. Before measuring ZP, the cell was thoroughly rinsed with ethanol and filtered water (0.2 µm pore sized syringe filter) using an appropriate syringe. A volume of 75 µl of sample was diluted with filtered water to 1 ml and added to the cell using a syringe. The number of runs set for each sample was 3.

4.3. Preparation of tryptic soy agar plates

Tryptic soy agar (TSA) plates were prepared by dissolving 16 g TSA in 400 ml distilled water. The solution was autoclaved before being distributed to sterile Petri dishes. The agar plates were left to cool on the bench overnight before being stored in the fridge at 4 °C.

4.4. Preparation of media and solutions

Tryptic soy broth

Tryptic soy broth (TSB) was prepared by dissolving 30 g TSB in 1000 ml distilled water. The solution was autoclaved.

TSB containing 1 % glucose

A 25 % (w/v) glucose solution was prepared by dissolving 25 g glucose in 100 ml distilled water. The solution was then sterile filtered and transferred to an autoclaved glass bottle. For the TSB containing 1 % glucose (TSB1%glu), 32 ml of 25 % (w/v) glucose was added to a sterile TSB solution, yielding a total volume of 800 ml.

Phosphate-buffered saline

The phosphate-buffered saline (PBS) was prepared by dissolving 8 g NaCl, 0.2 g KCl, 1.44 g Na_2HPO_4 and 0.24 g KH_2PO_4 (137, 2.7, 10 and 2 mM, respectively) in 800 ml of MILLI-Q H_2O (Sambrook and Russell, 2001). The pH was adjusted to 7.4 with 1 M NaOH before diluting the solution to a final volume of 1000 ml with MILLI-Q H_2O. Further, the solution was autoclaved.

0.9 % NaCl solution

The 0.9 % NaCl solution was prepared by dissolving 9 g NaCl in 1000 ml distilled water. The solution was then autoclaved.

Vancomycin solutions

The minimal inhibitory concentration (MIC) of vancomycin is known to be 2 µg/ml (1xMIC) (Moghadas-Sharif et al., 2014). The other concentrations used in the experiments were prepared in an increasing order as followed: 1xMIC, 10xMIC, 100xMIC and 1000xMIC, which corresponded to 2, 20, 200 and 2000 µg/ml, respectively.

A 50 mg/ml stock solution of vancomycin was prepared in a sterile MILLI-Q H_2O. After sterile filtration (using a 0.2 µm pore sized filter), the stock solution was diluted in sterile MILLI-Q

H_2O to obtain the concentrations of 5, 0.5 and 0.05 mg/ml. The different solutions (0.05, 0.5, 5 and 50 mg/ml) were further diluted in TSB1%glu to obtain the desired concentrations of 2, 20, 200 and 2000 µg/ml, respectively. The H2O:TSB1%glu ratio in the final concentrations was 1:25 (v/v).

4.5. Preparation of free NCE solutions

A 2 mM stock solution of NCE was prepared in TSB1%glu. The pH of the solution was adjusted to 7.4 with 1 M NaOH prior to sterile filtration (using a 0.2 µm pore sized filter). The stock solution was then diluted in TSB1%glu to obtain the desired concentrations of 1, 0.1 and 0.01 mM (Charnock, 2011). The NCE solutions were stored at 4 °C in the dark prior to each experiment for a maximum of 30 minutes. For each set of experiments, the solutions were freshly prepared.

4.6. Preparation of LCNPs containing NCE

The nanoparticles were prepared and analyzed as described above. Aliquots (2.5 ml) of the nanoparticle suspension were ultracentrifuged (165000 x g, 2 hours, and 10.0 °C) and the pellets resuspended in TSB1%glu. The nanoparticle suspension in TSB1%glu was further diluted with TSB1%glu to obtain the desired concentrations of 1, 0.1 and 0.01 mM NCE, respectively (Charnock, 2011). The nanoparticle suspensions were stored at 4 °C in the dark prior to each experiment for a maximum of 30 minutes. For each set of experiments, the solutions were freshly prepared. A suspension of empty nanoparticles in TSB1%glu was prepared under the same conditions, giving a concentration of 35 mg/ml.

4.7. Elimination of coagulase negative *Staphylococci* biofilm formation

The biofilm elimination assay was performed by a modified method originally described by Christensen et al. (1985).

4.7.1. Preparation of bacteria

To obtain inocula for the experiments, the strains were cultured on TSA at 37 °C for 24 hours. A single colony was cultured in 5 ml of TSB at 37 °C for 16-18 hours under rotational shaking

(225 rpm). After incubation, an aliquot of 1.5 ml was transferred to a sterile centrifugation tube and centrifuged for 7 minutes at 9500 x g. Further, the bacteria was resuspended in 0.9 % NaCl. The suspension was filtered (using a 5 µm pore size filter) and diluted with 0.9 % NaCl to make a resulting suspension that corresponded to $6x10^8$ colony forming units (CFU)/ml (2 McFarland solution). The 2 McFarland solution was freshly prepared prior to each experiment.

4.7.2. Biofilm formation

Suspensions of the strain were diluted with TSB1%glu to $6x10^6$ CFU/ml, and aliquots (50 µl) of the diluted bacterial suspensions were pipetted to sterile 96-well flat-bottomed polystyrene tissue culture plates and incubated for 24 hours at 37 °C. After incubation, the culture medium of each well was removed and the wells were washed twice (using a pipette) with an aliquot of 70 µl of sterile PBS to remove planktonic cells.

4.7.3. Photodynamic inactivation

We used three different treatments in our experiment:

A. NCE-PDT 1 (light irradiation dose of 37 J/cm^2)
B. NCE-PDT 2 (light irradiation dose of 90 J/cm^2)
C. NCE (NCE with no light irradiation).

Table 1 describes how the different solutions used in our experiment were plated on one 96-well plate (grey area). This plate setup was used for all three treatments. Two independent cell cultures of *S. epidermidis* RP62A were used.

The positive control was untreated biofilm, incubated with TSB1%glu.

Table 1: Template for the plating of the different solutions used in our experiment. Grey area denotes the 96-well plate.

Cell culture 1	Positive control (biofilm)	Empty NPs	NCE LCNPs 0.01 mM	NCE LCNPs 0.1 mM	NCE LCNPs 1 mM
			0.01 mM NCE	0.1 mM NCE	1 mM NCE
Cell culture 2	Positive control (biofilm)	Empty NPs	NCE LCNPs 0.01 mM	NCE LCNPs 0.1 mM	NCE LCNPs 1 mM
			0.01 mM NCE	0.1 mM NCE	1 mM NCE

An aliquot of 60 µl of each solution was pipetted on-to the plates into their respective wells and the plates was incubated in darkness at 37 °C for 6 (NCE-PDT 1 and NCE-PDT 2 groups) and 48 hours (NCE group). The NCE-PDT 1 and 2 groups were irradiated at 37 J/cm^2 and 90 J/cm^2, respectively, using the Aktilite® CL128 lamp, and incubated for 24 hours at 37 °C in darkness. The Aktilite® CL128 lamp is a red light source with a peak emission wavelength (λ_{em}) of approximately 630 nm.

A positioning of the lamp was done before the light irradiation was done as followed

- 37 J/cm^2 – the distance between the lamp and the plate was adjusted to 5 cm
- 90 J/cm^2 – the distance between the lamp and the plate was adjusted to 7 cm

Irradiation time for the two light irradiation doses was 8 minutes and 5 seconds for 37 J/cm^2, and 21 minutes and 27 seconds for 90 J/cm^2.

The light irradiation was performed in a dark room without windows.

4.7.4. Biofilm evaluation using crystal violet staining

When the plates were finished irradiated and incubated, they were washed three times with tap water and incubated overnight at room temperature (RT: 22 °C). After biofilm fixation, the adherent biofilm was stained with 0.1 % crystal violet (CV) (100 µl/well) and incubated at RT for 5 minutes. Excess stain was rinsed off by washing the plates with tap water. The 70 % (v/v) ethanol (150 µl) was added to each well before reading the optical density (OD) in an ELISA reader at 600 nm and single wavelength. The plates were shaken for 10 seconds before final reading.

4.7.5. Vancomycin

After biofilm formation by the method described in 4.7.2., aliquots of 60 µl of the different xMIC solutions (1, 10, 100 and 1000, respectively) were pipetted into their respective wells, as described below (**Table 2**). The positive control (untreated biofilm) and the blank (B: TSB1%glu only), were both incubated with a H_2O:TSB1%glu solution in the ratio 1:25 (v/v). The incubation time was 24 hours at 37 °C prior to washing and biofilm staining with 0.1 % crystal violet as described in 4.7.4.

Table 2: Template for the plating of the different vancomycin concentrations used for vancomycin testing. Grey area denotes the 96-well plate.

Cell culture 1	Positive control (biofilm)	TSB1%glu	Positive control (biofilm)	1xMIC	10xMIC	100xMIC	1000xMIC
Cell culture 2	Positive control (biofilm)	TSB1%glu	Positive control (biofilm)	1xMIC	10xMIC	100xMIC	1000xMIC

4.8. Statistical analysis

Untreated biofilm (positive control) was set as 100 % intact biofilm. Calculation of percentage of biofilm elimination was done by comparing to the untreated biofilm. All results are presented as the mean ± standard deviation (SD). Statistical analysis was performed using Student's *t*-test, and differences observed between results were considered to be statistically significant at $P < 0.05$.

5. Results and Discussion

5.1. Nanoparticle characterization

The pH of empty nanoparticle suspension and suspension of nanoparticles containing NCE (NCE LCNPs) was measured to be 4.47 and 2.56, respectively.

The determined size and polydispersity index, presented in **Table 3**, indicates that the nanoparticle suspensions (empty NPs and NCE LCNPs, respectively) have a relatively polydisperse nanoparticle size distribution. The nanoparticle size was expressed as NICOMP distribution. NICOMP distribution is a bimodal distribution where particles with similar size are grouped together in separate populations. Nanoparticles of a specific mean diameter size are then presented as a percentage (Andersen et al., 2013). The size distribution of nanoparticle suspensions used in this experiment showed a bimodal distribution with three specific size populations and a mean diameter was carefully selected as a representative value, as shown in **Table 3**. There were several small populations showing a mean size lower than 100 nm with a maximum percentage of 10. If not careful during the sample preparation for the size measurements, air bubbles can be formed on the inside of the tube wall and interfere with the measurements. Some of the populations showed a mean size higher than 500 nm with a percentage of approximately 50. This high percentage can reflect both the presence of large nanoparticles and nanoparticles that have aggregated.

The polydispersity index (PI) is a description of the nanoparticle size distribution. A high PI value denotes a wide size distribution while a low PI value denotes a narrow size distribution. The PI values for empty NPs (0.354 ± 0.011) and NCE LCNPs (0.426 ± 0.023) were acceptable. There was a significant difference in PI value between empty NPs and NCE LCNPs ($P < 0.05$).

Table 3: Particle size distribution and zeta potential for empty nanoparticles and nanoparticles containing NCE (n = 3).

Lecithin/chitosan nanoparticles	Mean diameter*		Polydispersity index	Zeta potential (mV)
	nm	%		
Empty	267.5	92.76	0.354 ± 0.011	5.34 ± 0.21
With NCE	253.4	95.71	0.426 ± 0.023	9.13 ± 0.35

*The mean diameter denote the representative value of NICOMP distribution

The lecithin/chitosan ratio was 20:1 (w/w) for both preparations, and the polydispersity index and zeta potential are presented as mean ± SD.

The determined values for the zeta potential (**Table 3**) indicate that the nanoparticles exhibited a slightly positive surface charge, which would indicate either the presence of chitosan on the outer surface of vesicles as lecithin is expected to be neutral and chitosan is known to have a positive charge (Andersen et al., 2013), or the partial presence of NCE on the outer surface.

The zeta potential (ZP) describes the overall surface charge properties of the nanoparticles, reflecting the nanoparticle's electrical potential (Barratt, 1999; Mohanraj and Chen, 2006). A negative ZP value denotes a negative charge and a positive ZP value a positive charge. Factors that influence the ZP value are the nanoparticle composition and the dispersion media. The stability of a nanoparticle suspension is affected by the ZP, showing good suspension stability at ZP values over +/- 30 mV due to electrostatic repulsion amongst the charged nanoparticles (Mohanraj and Chen, 2006). The electrostatic repulsion prevents aggregation of nanoparticles in the suspension. In addition to surface charge, the ZP value can be used to determine how a drug molecule interacts with the nanoparticle/drug carrier by either drug encapsulation in the nanoparticle center or drug adsorption to the nanoparticle surface (Barratt, 1999; Mohanraj and Chen, 2006).

As can be seen in **Table 3**, the ZP was significantly higher for the nanoparticles that contain NCE than the empty nanoparticles ($P < 0.05$).

During nanoparticle preparation, acetic acid was used as a solvent for chitosan. Acetic acid did also lower the pH, making the chitosan amino functional groups protonated and leading to a pH in the suspension of approximately 4.5 (4.47 for empty NPs). The high ZP value for NCE LCNPs can be contributed to both the NCE and the changes in pH of the solution. As stated earlier, the NCE is a derivative of 5-aminolevulinic acid, containing both an amine functional

group and a carboxylic group. At acidic pH, the amine functional group will be protonated, resulting in a positively charged NCE. The nanoparticles are formed by blending negatively/neutral charged lecithin with positively charged chitosan. When positively charged NCE is present along with the positively charged chitosan, the NCE has the opportunity to compete with the chitosan regarding electrostatic interaction with lecithin. This can result in nanoparticles comprised of lecithin, chitosan and NCE, yielding more free amino functional groups that are protonated in the chitosan molecule. This slightly higher density of positive charge of chitosan molecules in the nanoparticles can contribute to a higher positive surface charge, i.e. higher ZP value. The amount of free protonated NCE in the suspension can be a contributor to the low pH of 2.56.

In a study performed by Sonvico et al. (2006), they measured the density of lecithin/chitosan nanoparticles (1.175 g/cm^3) and compared it to lecithin alone (0.873 g/cm^3), suggesting that the formation of the NPs led to a more packed and denser structure than lecithin vehicles coated with chitosan.

The high ZP value can also be due to adsorption of the positively charged NCE to the nanoparticle surface, giving the nanoparticle an overall higher positive charge compared to the empty NPs. The exact explanation for the shift of the zeta potential on vesicle surface in the presence of NCE needs to be further elaborated and would be possible solved by using the labeled NCE.

Table 4: Entrapment of NCE in LCNPs as determined by ultracentrifugation method.

Drug (mg)	Entrapment efficiency (%)	Drug recovery (%)
100	23 ± 0.2	----*

*The amount of NCE in supernatant was not accessible

The low encapsulation efficiency (EE) presented in **Table 4** for NCE in LCNPs (23 ± 0.2 %) is probably due to the hydrophilic property of the NCE. Since the NCE is soluble in water, and the nanoparticle suspension is prepared in an aqueous environment, difficulties will arise during NCE incorporation. As described earlier, many hydrophobic drugs have been successfully incorporated into LCNPs such as progesterone (Sonvico et al., 2006), melatonin (Mrhar et al., 2009; Hafner et al., 2011) and glucocorticoids (Senyiğit et al., 2010). Sonvico et al. (2006) also

described the preliminary encapsulation experiments using the hydrophilic drug metoclopramide HCl, however, the results showed very low encapsulations (below 1 %). In this respect, our encapsulation efficiency was found to be acceptable to further evaluate the antimicrobial properties of the newly developed system.

5.2. Biofilm elimination assay

Before presenting the results for biofilm elimination, it is necessary to briefly explain the optimization process that led to the method described in chapter 4.7.

In this chapter, we will be dealing with the different term replicates in the results such as:

- Biological replicates: refers to independent cell cultures
- Replicates: refers to number of plates per independent cell culture
- Parallels: refers to number of wells per plate

5.2.1. Optimization of biofilm elimination method

We had decided to use the biofilm elimination method described by Christensen et al. (1985). This biofilm elimination method is currently applied as a screening method by the researchers and research groups at the Faculty of Health Sciences. Usually, this method is optimized for determination of the efficacy of antimicrobial agents against bacterial biofilm formed by e.g. *S. epidermidis*.

The optimized method also contained a bacterial strain that served as a negative control in addition to the biofilm-forming *S. epidermidis* ATCC35984 (RP62A 42-77). The negative control was *S. haemolyticus* 51-03, a clinical isolate that does not form biofilm. The negative control was already included in the biofilm elimination method at the very beginning of the experimental period.

In addition to the negative control, a blank control was also included in the method as a possible contamination control. The blank control did not contain biofilm, only TSB1%glu.

Experiment 1

In the first experiment, we decided to focus on the basic method of biofilm formation, biofilm elimination using an antimicrobial agent and biofilm evaluation using crystal violet dye. The antimicrobial agent we used was vancomycin, in the same concentrations and under the same conditions as described earlier. After this first biofilm elimination assay, we decided to include vancomycin as a standard comparison (control) throughout the entire experimental period.

Figure 14 shows intact *S. epidermidis* biofilm after the treatment with different concentrations of vancomycin. The results are the average from seven biological replicates during the whole experimental period. Treatment with 100xMIC and 1000xMIC vancomycin (200 µg/ml and 2000 µg/ml, respectively) showed a significant reduction of intact biofilm ($P < 0.05$) compared to 1xMIC and 10xMIC vancomycin (2 µg/ml and 20 µg/ml, respectively). There were no significant differences in biofilm treated with 100xMIC or 1000xMIC vancomycin solutions ($P > 0.05$).

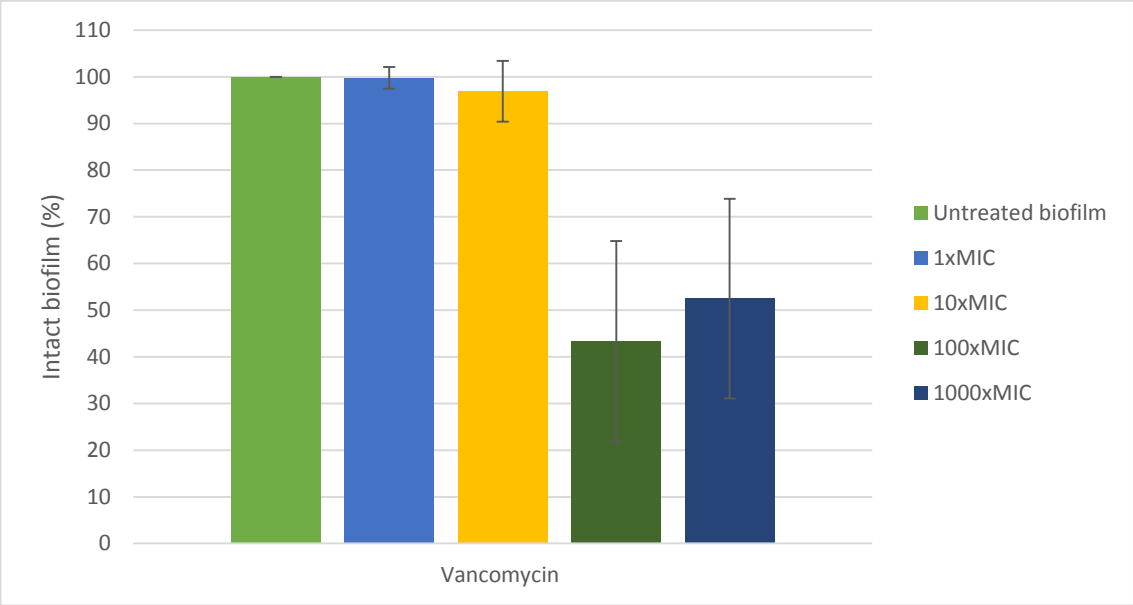

Figure 14: Intact *S. epidermidis* biofilm (%) after the treatment with vancomycin (mean ± SD, n = 7 biological replicates).

Experiment 2

When we started the biofilm elimination assay, we had little information about the NCE in respect to which concentration range we should focus on and what light doses we should use during the light irradiation. Due to this, we decided to base our choice on the published literature. As mentioned earlier, we already knew that NCE was a derivative of 5-ALA. Our search strategy was to find studies of 5-ALA-mediated PDT and the effect on bacterial biofilms, preferably *S. epidermidis* biofilm. A search in PubMed (February 2014), using the MeSH terms aminolevulinic acid, photodynamic therapy and biofilm, resulted in three articles. The most interesting article was written by Li et al. (2013), where they studied the effect of 5-ALA-mediated PDT on the antibiotic-resistant MRSA and MRSE biofilm.

At first, we decided to use 30, 40 and 50 mM NCE as an initial concentration range. The initial light dose was set to 37 J/cm^2. Solutions of NCE were minimally exposed to daylight and light from lamps in the ceiling during the entire experimental period. The exception was during the actual light irradiation. Light protection was achieved by covering the containers and plates with aluminum foil.

The free NCE in the concentration range mentioned above (30, 40 and 50 mM, respectively) were made in a TSB1%glu:H_2O-solution in a 50:50 (v/v) ratio. Since this was the first time we evaluated the biofilm elimination by applying PDT, we decided to use only one independent cell culture.

The biofilm elimination followed the basic method described in chapter 4.7., and the setup as described in **Table 5**.

Table 5: The different treatments used for biofilm elimination in experiment 2.

Treatment	Biological replicates	Light dose (J/cm^2)	Incubation time with NCE (hours)	Incubation time after light irradiation (hours)
A	1	37	24	24
B	1	0	48	----
C	1	0	48*	----

*Treatment C did not include any NCE, but the biofilm was incubated for 48 hours

The results presented in **Figure 15** show a significant reduction of intact biofilm for both treatment A and B ($P < 0.05$) with respect to the untreated biofilm (treatment C). Treatment B showed a significantly higher biofilm reduction as compared to A for all three concentrations ($P < 0.05$). This was rather unexpected, since treatment B did not involve light irradiation; we expected that NCE should not exhibit an effect on the biofilm when not exposed to light.

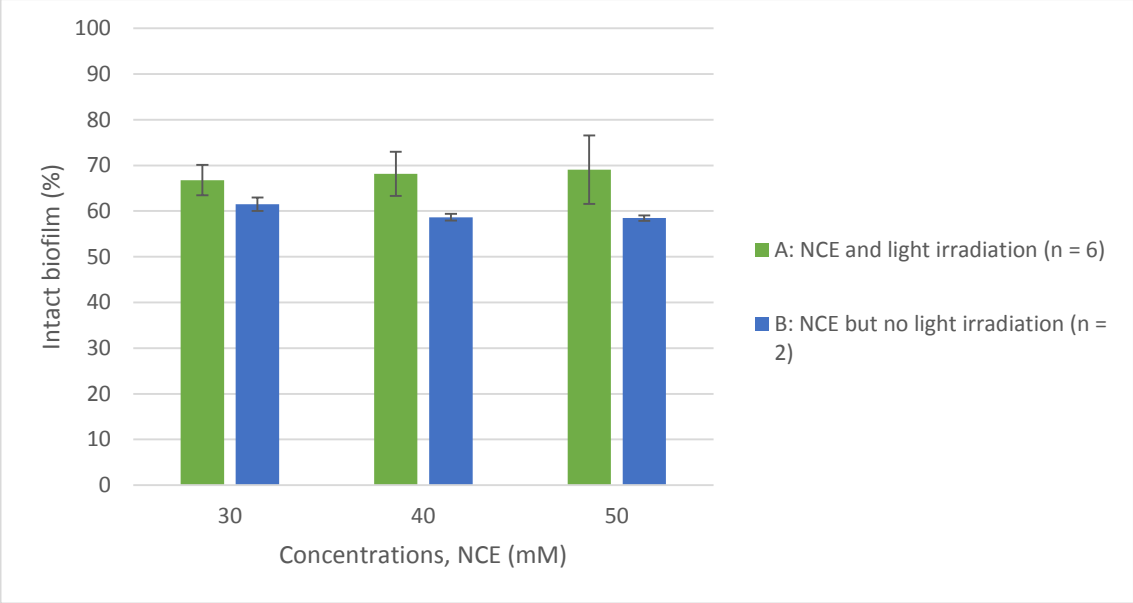

Figure 15: Intact *S. epidermidis* biofilm (%) after experiment 2 for A and B treatment (mean ± SD, n = replicates).

Experiment 3

To address rather surprising findings in the experiment 2, we modified the experimental setup to be as presented in **Table 6**. This experiment was a repetition of experiment 2, but with an increased number of biological replicates. The concentrations of NCE were 30, 40 and 50 mM, respectively.

Table 6: The different treatments used for biofilm elimination in experiment 3.

Treatment	Biological replicates	Light dose (J/cm^2)	Incubation time with NCE (hours)	Incubation time after light irradiation (hours)
A	3	37	24	24
B	3	0	48	----

The results in **Figure 16** show a significant reduction of intact biofilm for both treatments ($P < 0.05$) with respect to untreated biofilm (positive control). Group A showed a higher biofilm reduction compared to group B for all three concentrations, but the differences were not significant ($P > 0.05$). The NCE was still exhibiting an effect on the biofilm without the light irradiation.

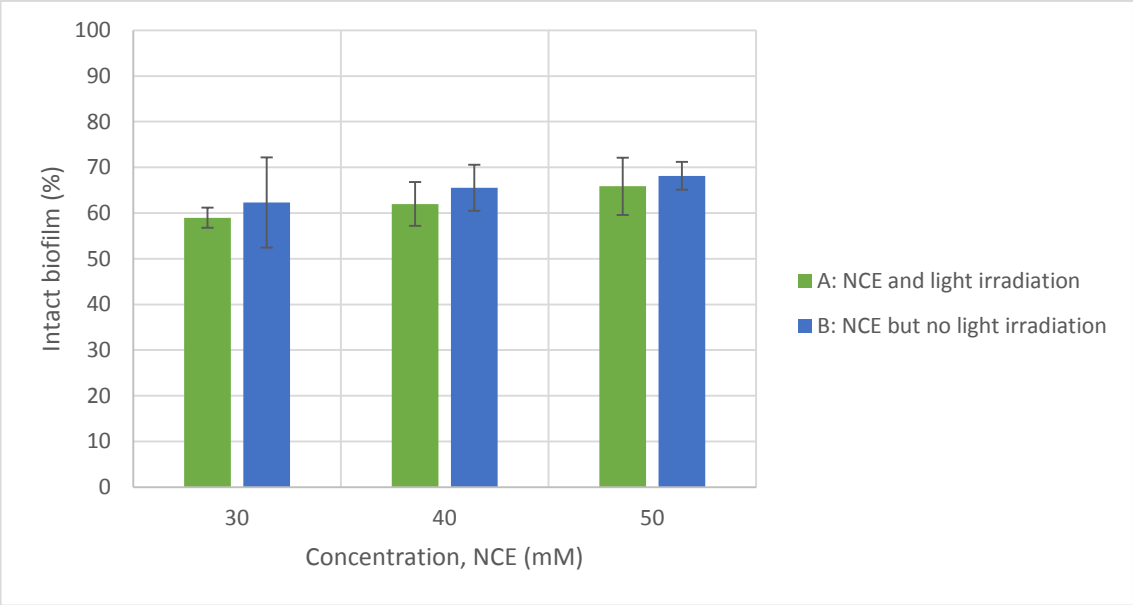

Figure 16: Intact *S. epidermidis* biofilm (%) after experiment 3 for treatment A and B (mean ± SD, n = 3 biological replicates).

Experiment 4

Before starting the experiment 4, we decided to exclude the negative control from the entire method. Excluding the negative control did not affect the biofilm elimination method since its only function was to act as a counterpart to the positive control, i.e. biofilm. Blank control was still included.

In this experiment, the concentration range for NCE was expanded by the addition of two lower concentrations, namely 10 and 20 mM. In addition, new time intervals for the incubation after the light irradiation were included. **Table 7** describes the full setup for the different treatments of biofilm used during the experiment 4.

Table 7: The different treatments used for biofilm elimination in experiment 4.

Treatment	Biological replicates	Light dose (J/cm^2)	Incubation time with NCE (hours)	Incubation time after light irradiation (hours)
A	1	37	24	1
B	1	37	24	3
C	1	37	24	24
D	3	37	24	24
E	3	0	24	----
F	3	0	48	----

Figure 17 shows the intact biofilm of *S. epidermidis* after the treatment with the groups A-C. The results show that there were no significant differences between the different time intervals (1, 3 and 24 hours, respectively) regarding the incubation after the light irradiation ($P > 0.05$). Only treatment B in the concentrations 30, 40 and 50 mM showed a significant reduction of intact biofilm ($P < 0.05$) with respect to untreated biofilm.

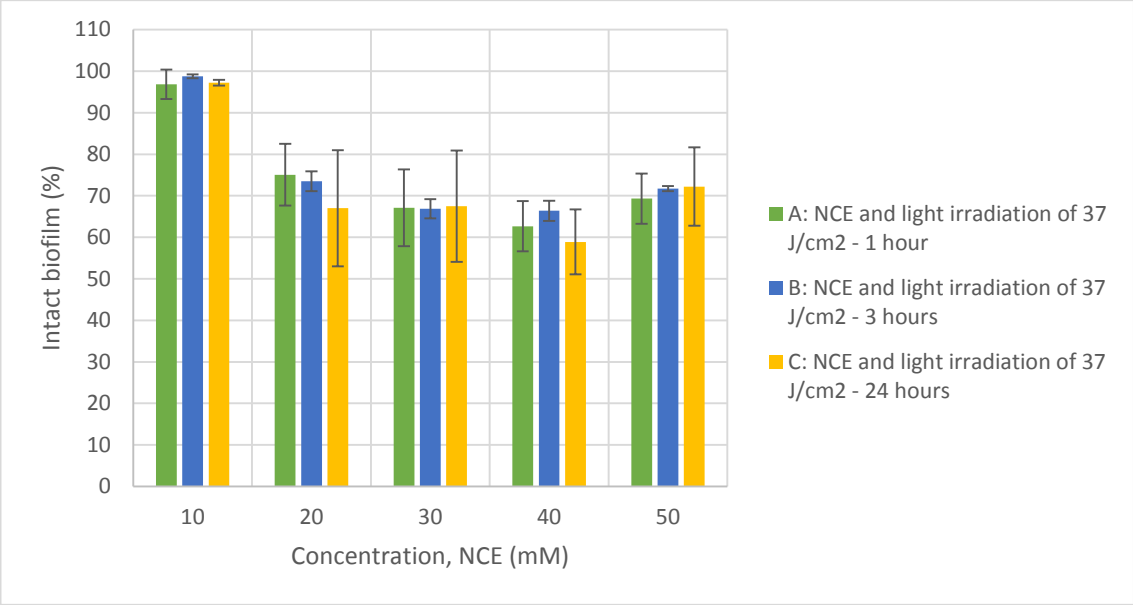

Figure 17: Intact *S. epidermidis* biofilm (%) after experiment 4 for treatment A-C (mean ± SD, n = 2 replicates).

The results for treatment D in **Figure 18** indicate significant reduction of intact biofilm for the concentrations 20, 30, 40 and 50 mM as compared to untreated biofilm ($P < 0.05$). Treatment E caused a significant reduction of intact biofilm in all concentrations ($P < 0.05$). Treatment F with 10 mM NCE did not induce significant reduction of intact biofilm.

Treatments E and F included NCE but without the light irradiation. This was used to assess the effect of NCE on the biofilm. The two treatments had different incubation time with NCE: 24 and 48 hours, respectively (**Table 7**). There was no significant difference between the treatments E and F ($P > 0.05$) although treatment E significantly reduced the intact biofilm. A high reduction of intact biofilm without the light irradiation can suggest that NCE has some toxic effect against the bacterial cells/biofilm at high concentrations. It would be interesting to perform some more toxicity testing to see if indeed 10 mM NCE is safe and non-toxic.

Both treatment B and D showed promising result regarding biofilm elimination, but treatment D was more reliable as the results comprised of three biological replicates as compared to one biological replicate for treatment B. Several more experiments have to be performed to determine the best time interval for incubation after the light irradiation. Further, we decided to use 24 hours as the final incubation time after the light irradiation.

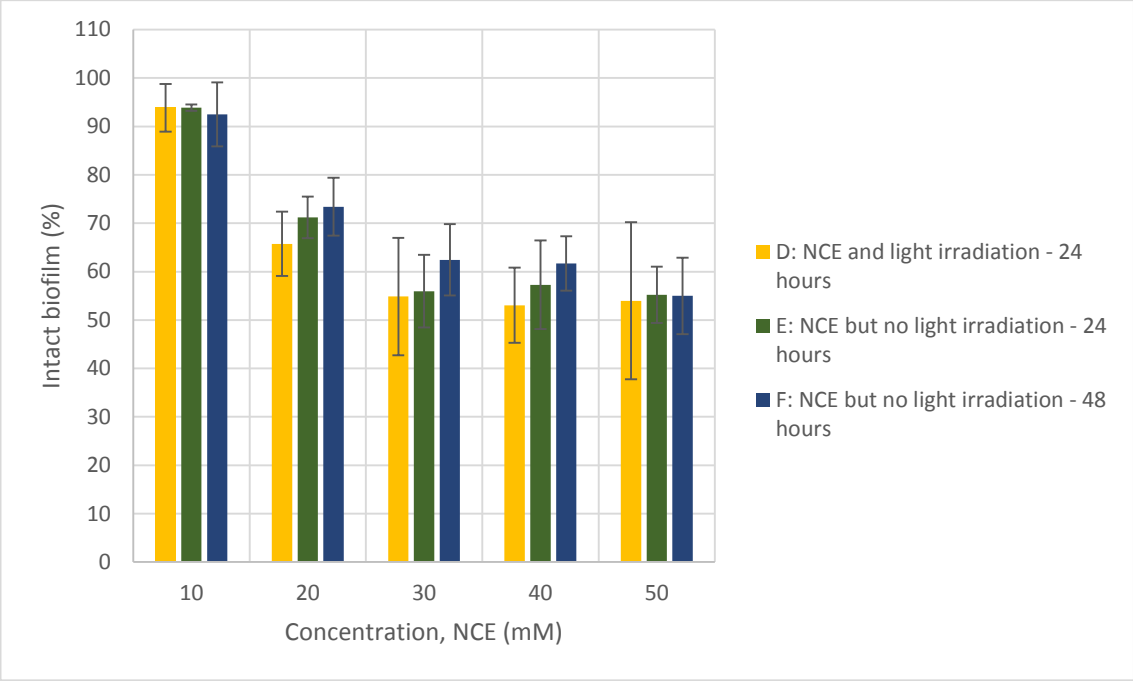

Figure 18: Intact *S. epidermidis* biofilm (%) after the treatments D-F (mean ± SD, n = 3 biological replicates).

Experiment 5

For this experiment, the concentration range of NCE was altered. The 50 mM concentration was excluded and a lower concentration of 5 mM was added instead. Also included was a new light dose of 90 J/cm^2 (Johnsson and Ramstad, 2003). **Table 8** shows the different treatments used.

Table 8: The different treatments used for biofilm elimination in experiment 5.

Treatment	Biological replicates	Light dose (J/cm^2)	Incubation time with NCE (hours)	Incubation time after light irradiation (hours)
A	3	37	24	24
B	3	90	24	24
C	3	0	24	----

Treatment A and B showed significant reduction of intact biofilm as compared to untreated biofilm ($P < 0.05$) for the NCE concentrations 10, 20, 30 and 40 mM (**Figure 19**). The differences in reduction of intact biofilm between the two treatments A and B (light irradiation of 37 and 90 J/cm^2, respectively) were not significant. Treatment C using 20, 30 and 40 mM NCE, respectively, where no light was used, showed a significant difference in intact biofilm reduction as compared to untreated biofilm ($P < 0.05$).

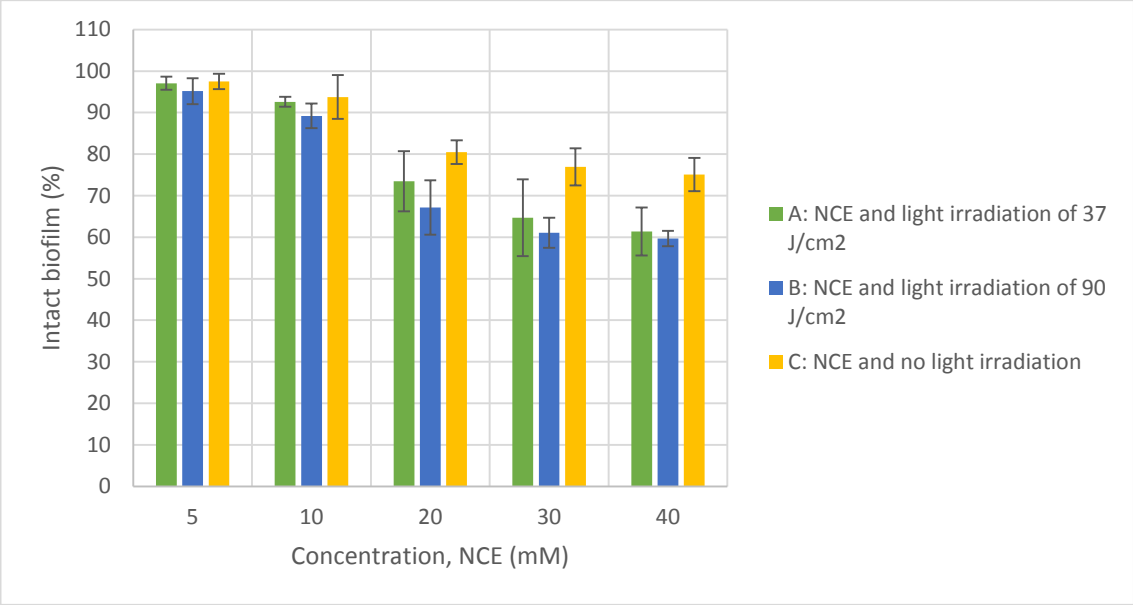

Figure 19: Intact *S. epidermidis* biofilm (%) after experiment 5 for treatments A-C (mean ± SD, n = 3 biological replicates).

The addition of 5 mM NCE and the results for treatment C supports the possibility of a toxic effect of NCE at concentrations higher than 10 mM. Although there was no significant difference between the two light irradiation doses for treatment A and B (37 and 90 J/cm^2, respectively), it would be interesting to do some more experiments using both doses since treatment B showed a slightly higher reduction of intact biofilm as compared to treatment A.

Experiment 6

The concentration range of NCE was the same as in experiment 5, and the setup for the different treatments is shown in **Table 9**.

Table 9: The different treatments used for biofilm elimination in experiment 6.

Treatment	Biological replicates	Light dose (J/cm^2)	Incubation time with NCE (hours)	Incubation time after light irradiation (hours)
A	1	37	24	24
B	1	90	24	24
C	1	0	24	----
D*	1	37	24	24

*Treatment D was applied using a black plate with clear lid and bottom (flat-bottomed)

Groups A-C showed no significant reduction of intact biofilm ($P > 0.05$) with respect to untreated biofilm (**Figure 20**). Compared to previous results in the experiments 2-5, treatment with NCE but without light irradiation (treatment C) showed no significant biofilm reduction, i.e. no toxic effect on bacterial cells/biofilm. The low reduction of intact biofilm was the wanted effect using NCE without light exposure. There can be several reasons why this effect was observed in this experiment and not earlier but some more experiments have to be performed to make a conclusion.

There was no significant difference between the light irradiation doses of 37 and 90 J/cm^2 (treatment A and B, respectively). Although there was an insignificant difference, the results for 37 J/cm^2 (treatment A) show a slightly higher biofilm reduction as compared to 90 J/cm^2 (treatment B), displaying an opposite effect as compared to the results for treatment A and B in the experiment 5. More experiments have to be performed for a reliable conclusion regarding the efficacy of the light irradiation doses.

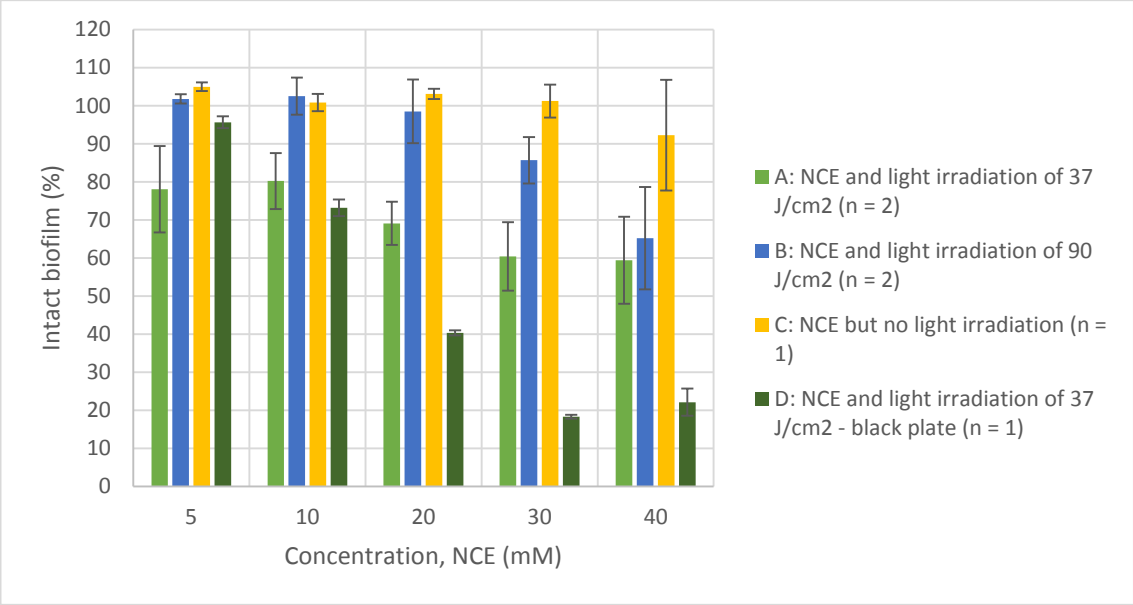

Figure 20: Intact *S. epidermidis* biofilm (%) after experiment 6 for treatments A-D, respectively (mean ± SD, n = replicates).

For the black plate, NCE concentrations of 10, 20, 30 and 40 mM showed a significant difference in reduction of intact biofilm ($P < 0.05$) with respect to untreated biofilm. Light scattering and the heat exchange during the irradiation can be one of the possible explanations. The color black absorbs all wavelengths of light and converts them into heat while the color white reflects all wavelengths, resulting in no heat conversion. This light scattering may also play a role in how much of the bacterial biofilm really undergoes light irradiation. The purpose of treatment D was just to evaluate whether there was any difference compared to the clear plates, however, more experiments need to be performed that include both clear and black plates and temperature measurements. To avoid a large deviation from the original biofilm elimination method, we decided to continue using the clear plates in further experiments.

We also tried to stain the biofilm with resazurin in addition to staining with crystal violet. Staining with crystal violet indicates the amount of overall biofilm biomass while staining with resazurin evaluates the biofilm viability (Ausbacher et al., 2014). Resazurin, with blue and non-fluorescent light, is reduced by metabolically active cells to resorufin, a pink fluorescent reaction product (Van den Driessche et al., 2014). We had some trouble with the staining method and the interpretation of the overall results, and due to limited time for the entire experiment, we decided to continue with CV-staining only. It would be interesting to include the resazurin staining as a step in the biofilm elimination method in the future.

The pH of all NCE solutions was measured. The concentrations ranged from 0.01 to 40 mM and the determined pH values from 6.83 to 3.29, respectively. Summarized, the pH becomes more acidic with higher NCE concentration, as expected.

Experiment 7

In this experiment, an additional time interval of 6 hours was included. The NCE concentration range was altered by excluding the higher concentrations over 10 mM, and including the concentrations 0.01, 0.1, 1 and 2 mM instead. A study executed for Photocure ASA reports that 0.1 and 1 mM NCE were highly effective against planktonic *S. aureus* (Charnock, 2011).

The biofilm elimination was performed using the treatments described in **Table 10**.

Table 10: The different treatments used for biofilm elimination in experiment 7.

Treatment	Biological replicates	Light dose (J/cm^2)	Incubation time with NCE (hours)	Incubation time after light irradiation (hours)
A	2	37	6	24
B	1	37	24	24
C	1	0	24	24

The results presented in **Figure 21** indicate a significant reduction of intact biofilm with 0.1, 1 and 2 mM NCE treatments after 6 hours incubation (A) and with 0.01, 0.1 and 5 mM NCE treatments after 24 hours incubation (B) with respect to untreated biofilm ($P < 0.05$). Group C exhibited no significant biofilm reduction ($P > 0.05$) with respect to untreated biofilm. For the NCE concentrations 0.01, 1 and 5 mM, treatment B exhibited a significantly higher reduction of intact biofilm as compared to treatment A ($P < 0.05$).

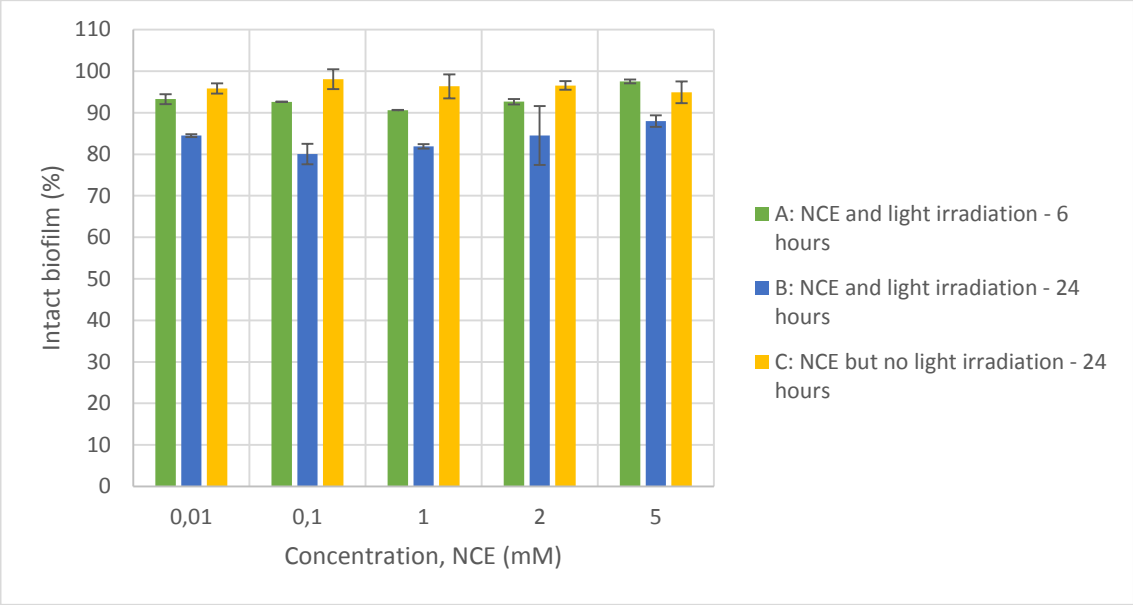

Figure 21: Intact *S. epidermidis* biofilm (%) after experiment 7 for treatments A-C (mean ± SD, n = 2).

The time intervals 6 and 24 hours for NCE incubation before the light irradiation (treatment A and B, respectively) showed some interesting results regarding the reduction of intact biofilm. The binding of a cationic molecules to the negatively charged bacterial cell membrane is a rapid process due to the driving electrostatic forces (Jori et al., 2006), resulting in a rapid diffusion through the bacterial membrane as compared to the slow uptake by mammalian cells that involve endocytosis (Sharma et al., 2012). Although different incubation times before light irradiation do not affect the amount of PS bound to microbial cells (Jori et al., 2006), we could clearly see, in this experiment, that 24 hours incubation with NCE before light irradiation was better than 6 hours. Further studies that include several time intervals are needed to draw a conclusion. We decided to use both time intervals during the rest of the experimentation period.

The planktonic growth of *S. epidermidis* was also measured. Growth curves for *S. epidermidis* were measured in both growth media (TSB1%glu:H_2O, 50:50 (v/v)) and different NCE concentrations (0.01, 0.1, 1, 5 and 10 mM). The growth curves were measured in an ELISA reader using a 96-well polystyrene tissue culture plate. For the growth of *S. epidermidis* in growth media (**Figure 22**), a planktonic cell suspension in growth media ($6x10^6$ CFU/ml) were pipetted to a 96-well polystyrene tissue culture plate. The plate was incubated in the ELISA reader for 18-24 hours and the optic density at 650 nm (OD_{650}) was measured every 20 minutes. The planktonic cell suspension was grown under dynamic conditions with shaking of the plate

during incubation. The time interval for shaking was approximately 17 minutes before every read.

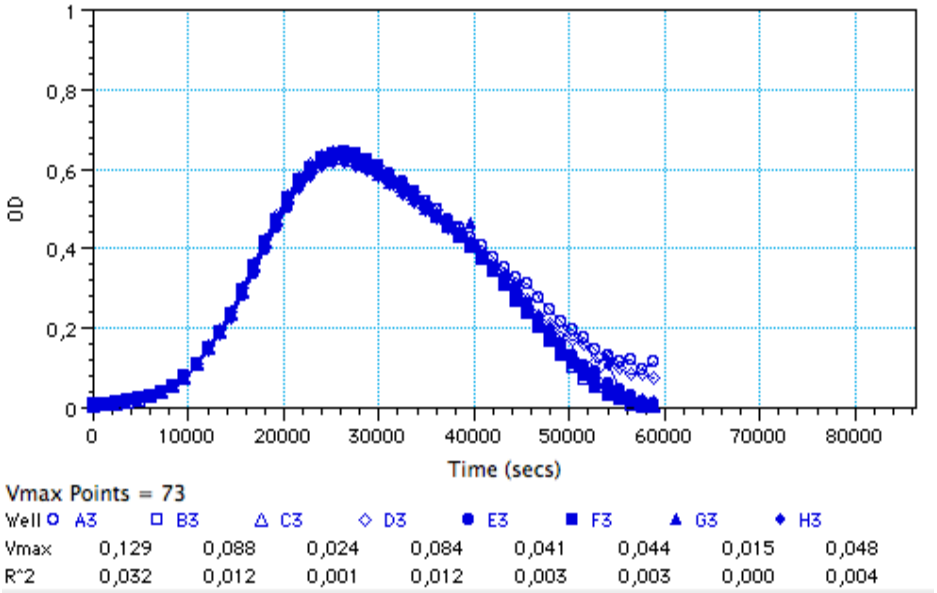

Figure 22: Growth curve of *S. epidermidis* planktonic cells in growth media under dynamic conditions (OD = optical density at 650 nm).

The growth of *S. epidermidis* planktonic cells in growth media (TSB1%glu:H_2O, 50:50 (v/v)) was found to be not optimal. When looking at the growth curve (**Figure 22**), we can see that the cells grow to a certain point (OD ≈ 0.6) before they die. This is not a typical bacterial growth curve. A bacteria growing under the right conditions exhibit five distinct phases of growth, namely (a) lag phase – a delay before growth, (b) exponential phase – a rapid cell division, (c) stationary phase – the cells don't replicate, (d) death phase – loss of cell viability, and (e) long-term stationary phase (Rolfe et al., 2012). In our growth curve, we can see that the cells were growing and dying, but we could not detect the stationary phase. This lack of stationary phase can indicate suboptimal growth conditions. The growth media comprised of both TSB1%glu and H_20 in a 50:50 ratio (v/v). TSB1%glu provides the nutrition necessary for bacterial growth, and by diluting this solution 50:50 (v/v) with H_2O, the nutrition will be reduced, resulting in less nutrition available for bacterial growth.

For the growth curve of *S. epidermidis* in different NCE concentrations (**Figure 23**), a planktonic cell suspension was added to NCE solutions (with concentrations 0.01, 0.1, 1, 5 and 10 mM) prepared in growth media (TSB1%glu:H_2O, 50:50 (v/v)). The suspensions with NCE were pipetted to a 96-well polystyrene tissue culture plate. The plate was incubated in the ELISA reader for 18-24 hours and the optical density at 650 nm (OD_{650}) was measured every 20 minutes. The NCE suspensions were grown under dynamic conditions with shaking of the plate during incubation. The time interval for shaking was approximately 17 minutes before every read.

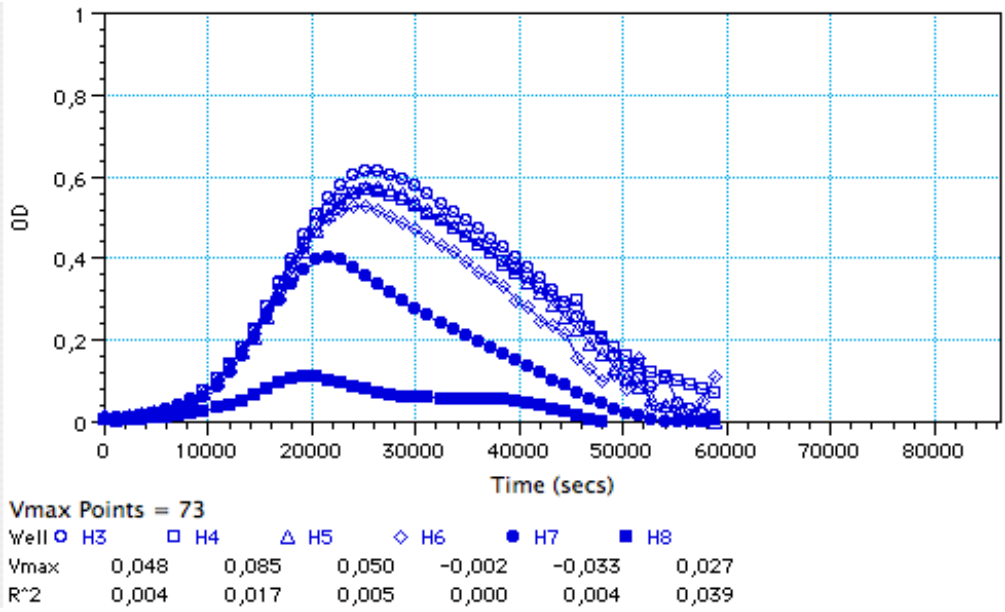

Figure 23: Growth curve of *S. epidermidis* in the presence of NCE concentrations in the range 0.01, 0.1, 1, 5 and 10 mM (H4, H5, H6, H7 and H8, respectively) under dynamic conditions (OD = optical density at 650 nm).

The growth curve in **Figure 23** confirms the results for the growth curve for *S. epidermidis* planktonic cells in growth media only (**Figure 22**). There was still a lack of stationary phase. In addition, the presence of NCE in higher concentrations such as 5 and 10 mM (H7 and H8, respectively) made the conditions for bacterial growth even poorer. This phenomenon can be a result of the low pH in the solution due to high concentration of NCE, as described earlier. Nostro et al. (2013) studied the effect of growth media of pH 5.0 and 6.0, respectively, on *Staphylococcal* growth and biofilm formation. The results demonstrated a reduction in growth and biofilm formation. They concluded that the inhibition was related to pH value and the type

of acidulant. These results can possibly explain the poor bacterial growth in the presence of 5 and 10 mM NCE we have observed.

Experiment 8

The focus of this experiment was to optimize the bacterial growth for both planktonic cells and biofilm by increasing the amount of nutrients available in growth medium. The pH was also altered in the different NCE concentrations.

The growth of *S. epidermidis* planktonic cells (**Figure 24**) in the presence of different NCE concentrations (0.01, 0.1, 1 and 5 mM) was measured using the same method as described for growth curves in experiment 7. For optimal nutrition, the different NCE concentrations were made in TSB1%glu alone, and the pH for each concentration was determined and adjusted to approximately 7.4 with 1 M NaOH. The cell suspensions were grown under static conditions with no shaking of the plate during incubation. The only exception was a 5 second time interval of shaking before every read.

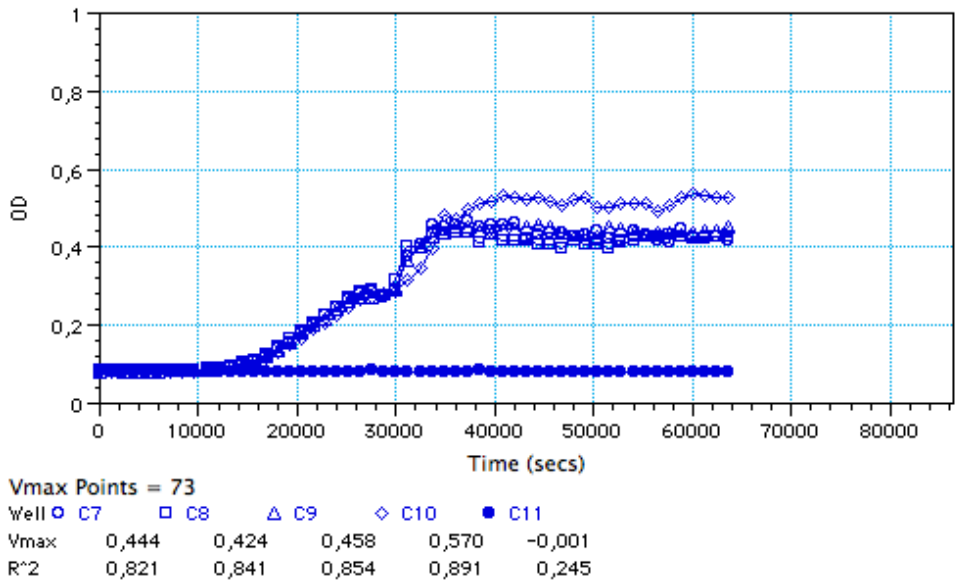

Figure 24: Growth curve of *S. epidermidis* planktonic cells in the presence of different NCE concentrations in the range 0.01, 0.1, 1 and 5 mM (C8, C9, C10 and C11, respectively). C7 is growth media alone (OD = optical density at 650 nm).

After adjusting the pH of the NCE concentrations, and supplying enough nutrients by using TSB1%glu as growth media, the *S. epidermidis* planktonic cells reached a stationary phase, exhibiting a typical bacterial growth curve (**Figure 24**).

The planktonic cells did not grow at all in 5 mM NCE even though the pH was adjusted to approximately 7.4. This can suggest that the NCE in high concentrations may be toxic to the bacterial cells. This finding need to be further explored.

The growth of *S. epidermidis* biofilm was measured using the same method described in experiment 7. The growth media was TSB1%glu, and the biofilm was grown under static conditions.

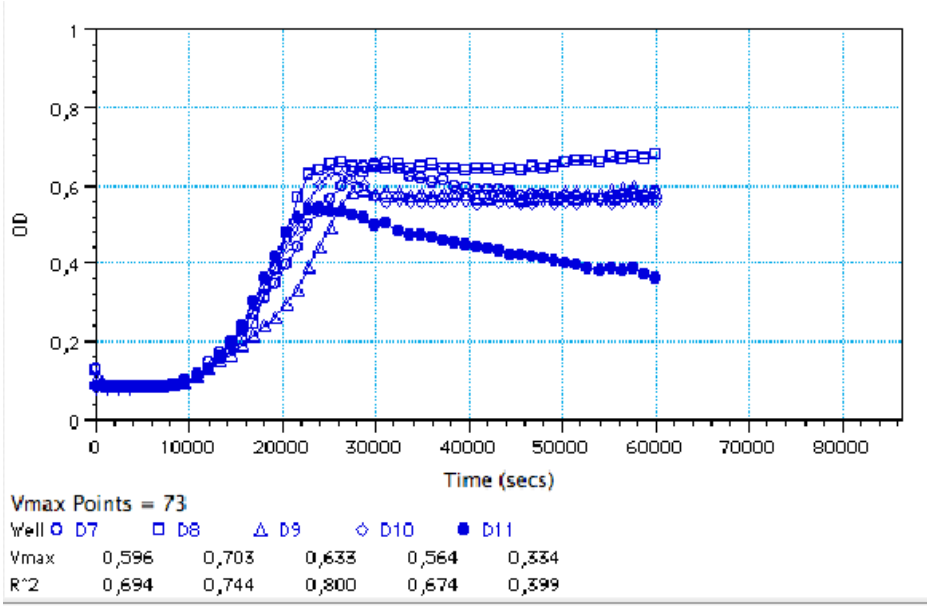

Figure 25: Growth curve of *S. epidermidis* biofilm in growth media under static conditions (OD = optical density at 650 nm).

The growth curve of *S. epidermidis* biofilm (**Figure 25**) exhibited the same pattern as planktonic cell growth (described above). The bacterial cells reached a stationary phase after exponential growth. When comparing the growth of biofilm with planktonic cells, we can see that the optical density (OD) is higher for biofilm than for planktonic cells (≈ 0.6 and ≈ 0.5, respectively).

The growth of *S. epidermidis* biofilm was additionally measured under dynamic conditions that resulted in a poor biofilm formation. This finding has been also reported in a study performed

by Stepanović et al. (2001) where they concluded that *S. epidermidis* biofilm formation was significantly reduced under dynamic conditions.

The growth of biofilm over 72 hours using CV staining was also measured (**Figure 26**). Biofilm growth and formation were conducted under the same conditions as stated earlier. NCE was not included.

Three treatment points were included, namely (a) 24 hours, (b) 48 hours, and (c) 72 hours, respectively.

24 hours: after 24 hours, the biofilm was washed with PBS.

48 hours: after 24 hours, the biofilm was washed with PBS before new growth media was added. The biofilm was incubated for another 24 hours before it was washed with tap water.

72 hours: after 24 hours, the biofilm was washed with PBS before new growth media was added. The biofilm was incubated for another 48 hours before it was washed with tap water.

After the final washing for each treatment point, the biofilm was set to fixate before CV staining and measurement of optical density at 600 nm (OD_{600}) was performed.

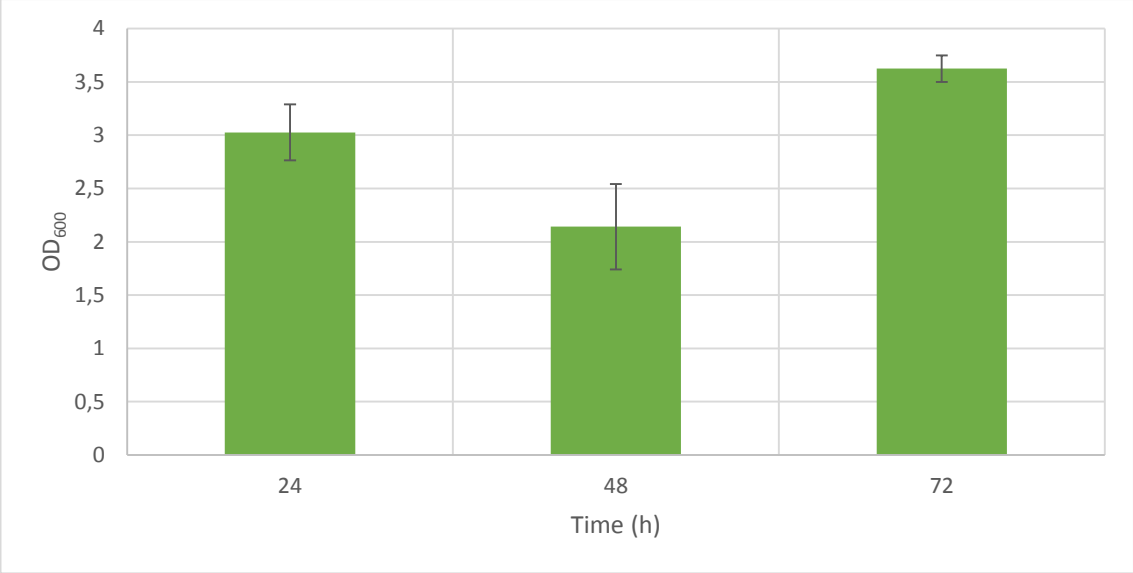

Figure 26: Growth of *S. epidermidis* biofilm in TSB1%glu after 24, 48 and 72 hours (mean ± SD, n = 2 biological replicates).

Biofilm growth after 48 hours was significantly decreased compared to growth after 24 hours ($P < 0.05$). For the 48-hour treatment, the planktonic cells were rinsed off, and new growth media was added to the biofilm. The removal of planktonic cells may have an impact on the biofilm growth when it comes to the recruitment of planktonic cells. The 72-hour treatment had a significantly higher OD_{600} compared to both the 24 and 48 hour group ($P < 0.05$).

These results for biofilm growth indicated that bacteria within the biofilm were able to reproduce under optimal conditions. In addition, the reduced nutrition did not affect the biofilm growth after the initial biofilm formation.

Experiment 9

This experiment was a repetition of experiment 7, but with an optimized growth condition for *S. epidermidis* biofilm. The concentration range of NCE was the same (0.01, 0.1, 1, 2 and 5 mM, respectively), but the solutions were made in TSB1%glu alone and pH was adjusted to approximately 7.4.

Table 11 shows the setup for the different treatments, where F is empty nanoparticles. The suspension with empty nanoparticles was made as described in chapter 4.6., giving a concentration of 49 mg/ml empty nanoparticles in TSB1%glu. The pH was measured to be in the range 7.0-7.5.

Table 11: The different treatments used for biofilm elimination in experiment 9.

Treatment	Biological replicates	Light dose (J/cm^2)	Incubation time with NCE (hours)	Incubation time after light irradiation (hours)
A	2	37	6	24
B	2	37	24	24
C	2	90	6	24
D	2	90	24	24
E	2	0	48	----
F*	2	0	24*	----

*Treatment F was empty NPs without any NCE, but the incubation time was 24 hours

The effect of empty nanoparticles on biofilm was also tested. As described earlier, chitosan exhibits antimicrobial effect through several mechanisms of action. One proposed mechanism includes the binding to negatively charged cell walls and membranes (Pelgrift and Friedman, 2013). Since the NPs have a positive surface charge (ZP) due to the chitosan, it was interesting to see if the NPs had an effect on the negatively charged biofilm matrix as an empty carrier system.

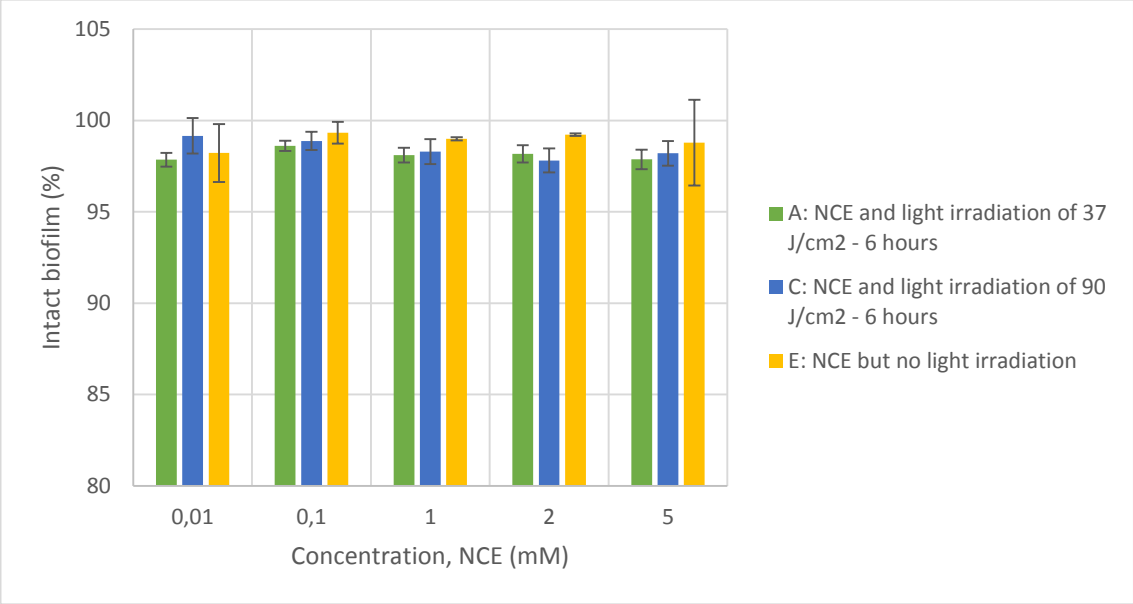

Figure 27: Intact *S. epidermidis* biofilm (%) after treatment A, C and E (mean ± SD, n = 2 biological replicates).

The results presented in **Figure 27** showed no significant difference in reduction of intact biofilm between treatment A and C (37 and 90 J/cm^2, respectively) for 6 hours incubation with NCE before light irradiation ($P > 0.05$). Treatments A and C exhibited no significant reduction of intact biofilm with respect to untreated biofilm. For treatment E (NCE but no light irradiation), 1 and 2 mM NCE concentrations showed a significant reduction of intact biofilm ($P < 0.05$) with respect to untreated biofilm. In previous experiments, the results from treatments with NCE but no light irradiation have indicated that NCE may be toxic for bacterial cells and biofilm at concentration 5 mM and higher. This treatment can indicate that NCE may be toxic at even lower doses, however, this has to be explored further.

In **Figure 28**, the 5 mM NCE concentration in treatment D showed a significant reduction of intact biofilm ($P < 0.05$) with respect to untreated biofilm. There was no significant difference in reduction of intact biofilm between B and D (37 and 90 J/cm^2, respectively) for 24 hours incubation with NCE before light irradiation.

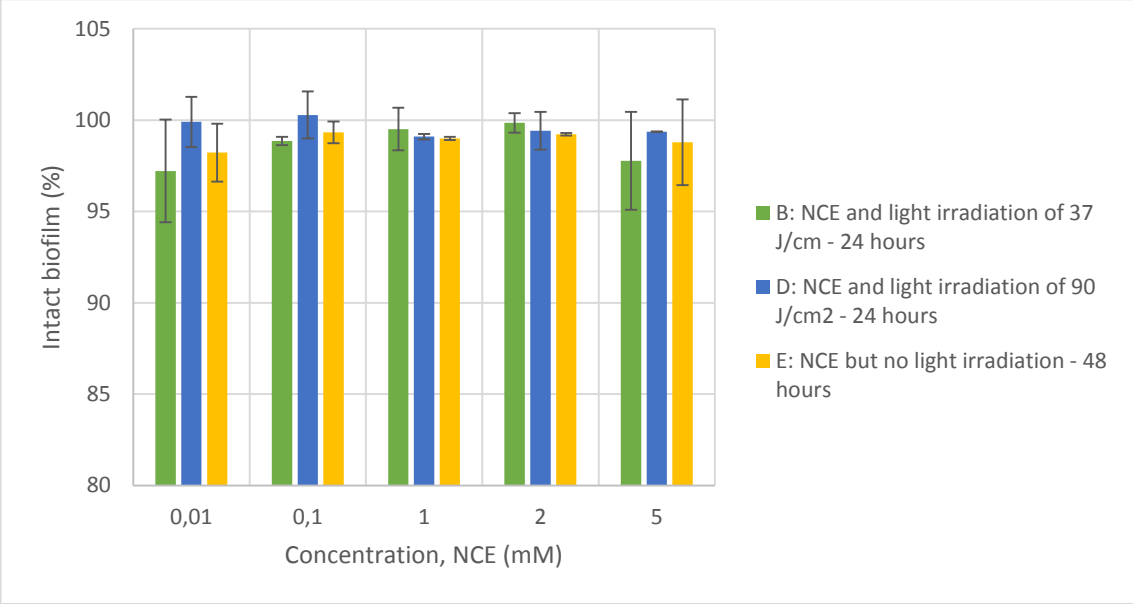

Figure 28: Intact *S. epidermidis* biofilm (%) after treatment with B, D and E (mean ± SD, n = 2 biological replicates).

The reduction of intact *S. epidermidis* biofilm after the optimization of bacterial cell growth was found to be lower, compared to the biofilm reduction before optimization. Before the pH and nutrition availability were optimized, the bacteria grew rapidly before they died (**Figure 22** and **Figure 23**), suggesting that the bacteria were already dying when the NCE-mediated PDT was applied, resulting in a higher reduction of intact biofilm. In addition, there was no evidence suggesting that the high reduction of intact biofilm was an effect of the NCE-mediated PDT treatment. The biofilm reduction may have been a result of possible NCE toxicity.

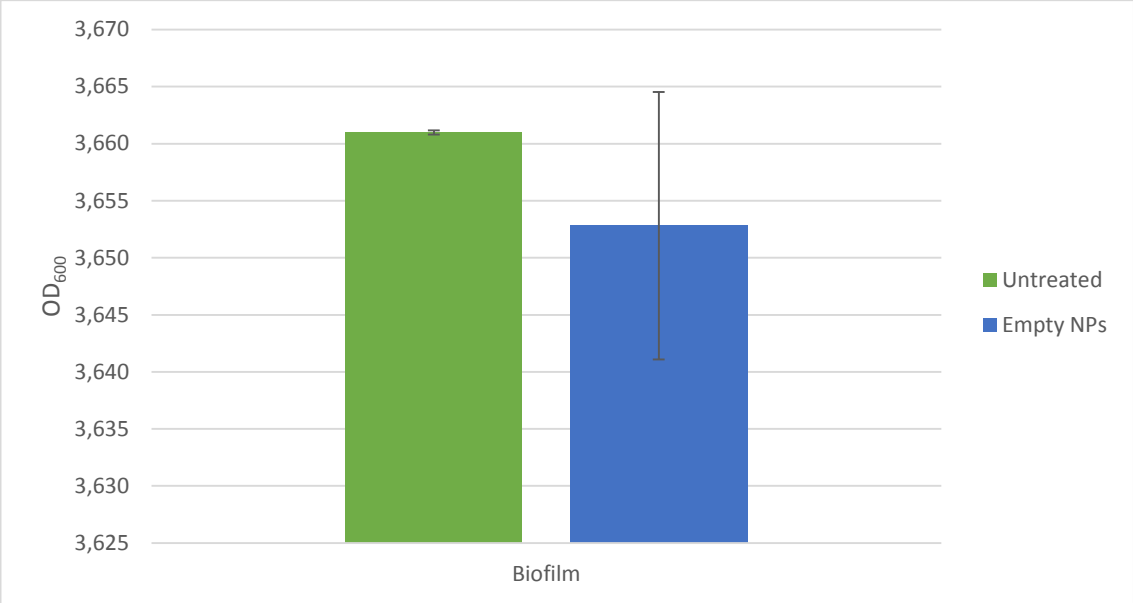

Figure 29: The difference between untreated biofilm and biofilm treated with empty nanoparticles (NPs) (mean±SD, n=2 biological replicates).

There was no significant reduction in OD_{600} for biofilm treated with empty NPs compared to untreated biofilm (**Figure 29**). From these results, it seems that the positively charged LCNPs did not have an effect on *S. epidermidis* biofilm. As mentioned earlier, chitosan is a weak base with pKa value ranging between 6.2-7 (Wong, 2009). In solutions with a pH value higher than the pKa, the amino functional group will be neutral. The amino functional group will be protonated, yielding a positive charge, when the pH is lower than the pKa. In our nanoparticle suspension, the pH was measured to be in the range 7.0-7.5, probably contributing to the charge being more neutral than positive, hence the low surface charge (ZP) of approximately 5 mV. This can be one of the factors affecting the biofilm reduction. The other factor can be the availability of free amino functional groups in chitosan molecules and on the nanoparticle surface. As described earlier, the lecithin/chitosan nanoparticles are self-assembled due to an electrostatic interaction between chitosan and lecithin (Sonvico et al., 2006). The availability of free functional amino groups reduces during the formation of these interactions. A higher density of positive charged chitosan will bind stronger and more frequent to cell walls and membranes compared to a less positive charge density (Kong et al., 2010; Pelgrift and Friedman, 2013). In this situation, the degree of deacetylation (DD) plays an important role, since this value represents the proportion of amine functional groups that are deacetylated, i.e. free amino functional groups (Berger et al., 2004).

Zhang et al. (2013) studied the effect of streptomycin conjugated with chitosan on *Listeria monocytogenes* biofilm. The streptomycin-chitosan conjugate showed an effective killing of bacteria and eradication of established biofilm compared to streptomycin alone. This conjugate proved to be effective against other Gram-positive bacteria such as *S. aureus*, but not against Gram-negative bacteria such as *P. aeruginosa*. The authors concluded that chitosan, with its polycationic property, contributed to a more efficient delivery of streptomycin into biofilms formed by Gram-positive bacteria. The use of chitosan made the biofilm more susceptible to lower doses of streptomycin.

Shrestha et al. (2014) studied the efficacy of chitosan nanoparticles with rose bengal (CRSB) combined with PDT against 21-day-old *Enterococcus faecalis* biofilms. Complete biofilm elimination, reduced biofilm thickness and complete disruption of biofilm architecture was observed after CRSB PDT treatment as compared to free rose bengal. They concluded that increased uptake of CSRB nanoparticles was mainly attributed to the particle's positive charge and nano-size of the system assuring the stronger interactions with bacterial cell and the negatively charged biofilm matrix.

During the light irradiation, we also measured the temperature in the area. An increase in temperature of 1.5 and 2.2 °C was measured for the light doses 37 and 90 J/cm^2, respectively. This was just a control measurement to evaluate whether an increased temperature could interfere with the effect of light irradiation. The results were not interesting for further examination.

To summarize; during the experiments 2-9, the biofilm elimination method and the bacterial growth were optimized according to the points stated below:

- Concentrations of NCE should be in the range of 0.01, 0.1 and 1 mM; higher concentrations might be toxic to bacteria
- pH of the NCE solutions should be approximately 7.4; the preferred pH for optimal bacterial growth
- The amount of nutrition in growth media is sufficient when using TSB1%glu without too much H_2O
- Light doses of both 37 and 90 J/cm^2 are applicable
- Biofilm elimination with vancomycin as a model antibiotic showed the same trend for each biological replicate, making it a good standard

5.2.2. NCE-mediated PDT of *S. epidermidis* biofilm

Concentrations of NCE used in this final experiment were 0.01, 0.1 and 1 mM, and the experimental setup is described in **Table 12**.

Table 12: The different treatments used for NCE-mediated PDT of *S. epidermidis* biofilm.

Treatment	Biological replicates	Light dose (J/cm^2)	Incubation time with NCE (hours)	Incubation time after light irradiation (hours)
A	2	37	6	24
B	2	90	6	24
C	2	0	48	----

After preparation of nanoparticle suspensions containing 0.01, 0.1 and 1 mM NCE (NCE LCNPs), the pH was measured, exhibiting a pH ranging from 7.0 to 7.5. Due to the low entrapment of NCE in the LCNPs, the different NCE LCNP suspensions were prepared using the same stock suspension (as described in chapter 4.6.) When using the same stock suspension for the preparation of the different NCE concentrations (0.01, 0.1 and 1 mM), the concentration of nanoparticles will not be identical for the different suspensions. In this experiment, the amount of LCNPs (mg) per volume TSB1%glu (ml) was 1.106, 11.06 and 110.6 mg/ml, respectively.

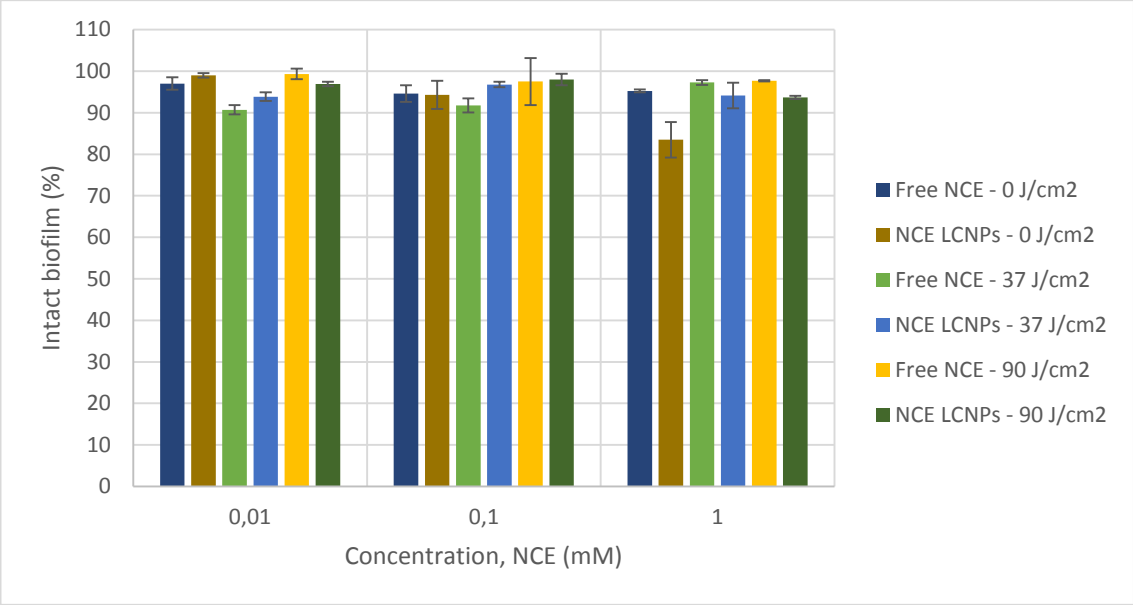

Figure 30: Intact *S. epidermidis* biofilm (%) after experiment 10 (mean ± SD, n = 2 biological replicates).

Figure 30 shows the results after the treatments A-C. Free NCE in the concentration 0.01 mM exhibited a significant higher reduction of intact biofilm with the light irradiation dose of 37 J/cm^2 (treatment A) as compared to 90 J/cm^2 (treatment B) ($P < 0.05$). Treatment A, with 0.01 mM NCE LCNPs showed a higher biofilm reduction as compared to treatment C, respectively ($P < 0.05$). The biofilm reduction with treatment C and 1 mM free NCE was significantly higher as compared to treatment A and 1 mM free NCE ($P < 0.05$), but for 0.01 mM free NCE, the reduction with treatment A was significantly higher as compared to treatment C ($P < 0.05$).

Empty NPs, 0.01 and 1 mM NCE LCNPs and 1 mM free NCE showed significant reduction of intact biofilm ($P < 0.05$) with respect to untreated biofilm when using the light irradiation dose of 37 J/cm^2 (**Figure 31**). There was a significant difference in biofilm reduction for 1 mM NCE LCNPs as compared to free NCE ($P < 0.05$). There were no significant differences between empty NPs and 0.1 mM NCE LCNPs and 0.01 and 0.1 mM free NCE, respectively.

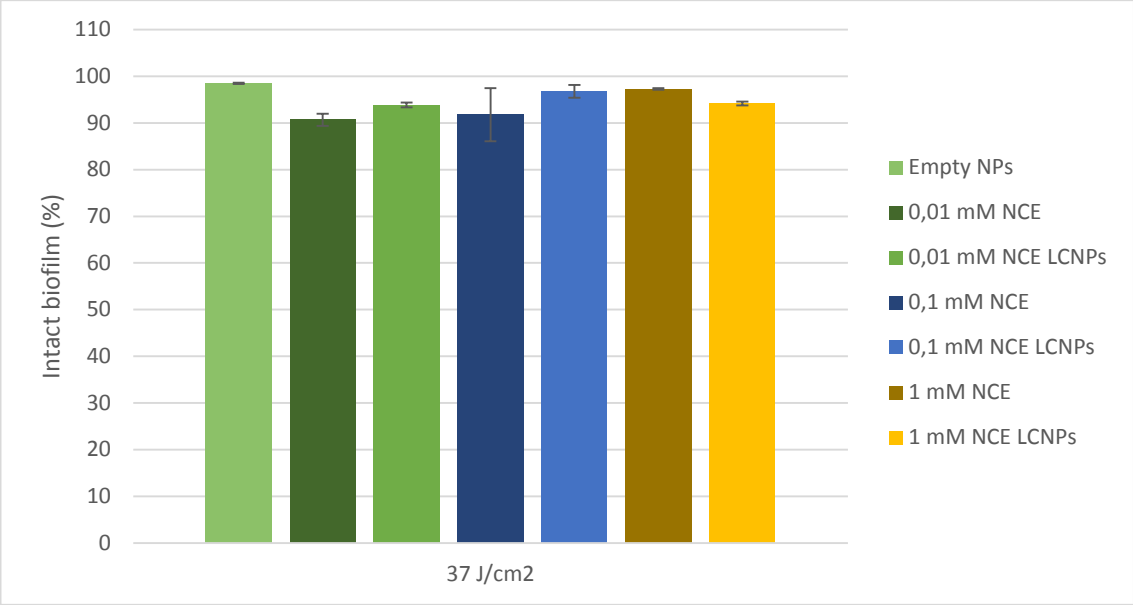

Figure 31: Intact *S. epidermidis* biofilm (%) after PDT with NCE applying 37 J/cm^2 light source (mean ± SD, n = 2 biological replicates).

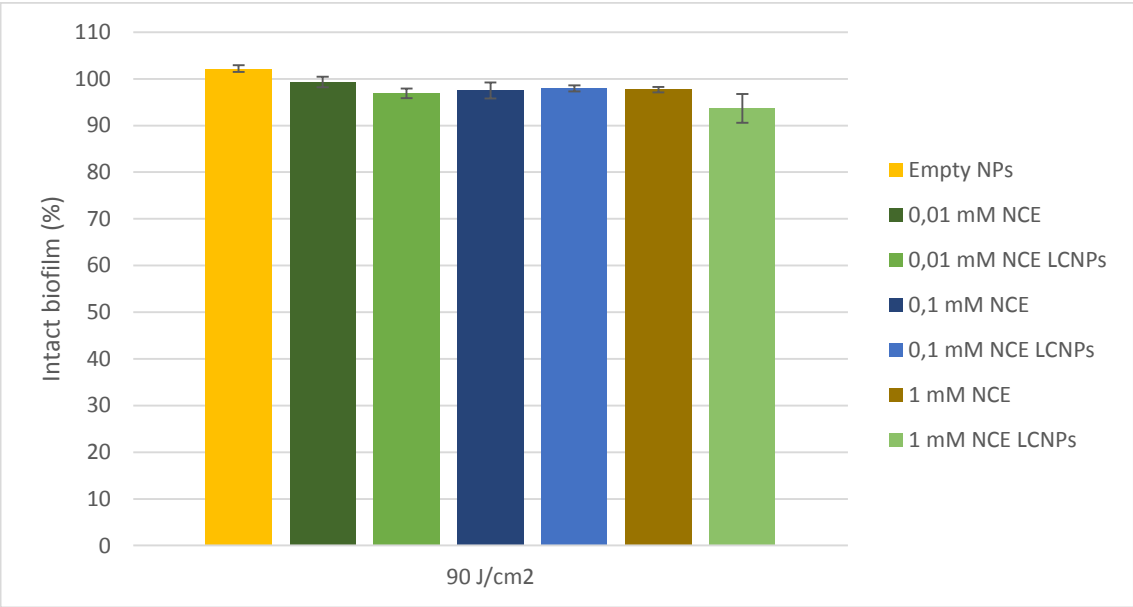

Figure 32: Intact *S. epidermidis* biofilm (%) after PDT with NCE applying 90 J/cm^2 light source (mean ± SD, n = 2 biological replicates).

All treatments showed no significant reduction of intact biofilm ($P > 0.05$) with respect to untreated biofilm when using the light irradiation dose of 90 J/cm^2 (**Figure 32**). Empty NPs showed no significant increase/reduction of intact biofilm with respect to untreated biofilm.

NCE LCNPs (0.01 and 0.1 mM) and free NCE (1 mM) exhibited a significantly higher biofilm reduction as compared to empty NPs ($P < 0.05$)

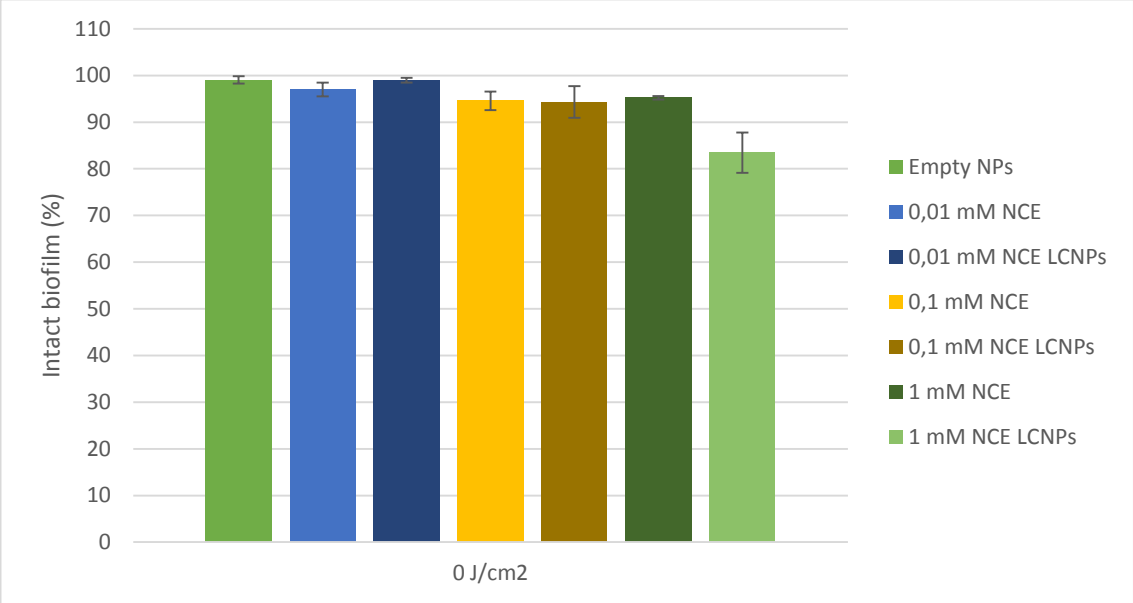

Figure 33: Intact *S. epidermidis* biofilm (%) after PDT with NCE and no light irradiation (mean ± SD, n = 2 biological replicates).

Free NCE in the concentration 1 mM showed a significant reduction of intact biofilm ($P < 0.05$) with respect to untreated biofilm (**Figure 33**). There was a significant difference between 1 mM free NCE and empty NPs regarding reduction of intact biofilm ($P < 0.05$). The expected results after treatment C was no reduction of intact biofilm since this treatment involved NCE alone without the light irradiation. The results presented above in **Figure 33** exhibits expected effect for the lowest NCE concentrations, for both free NCE and NCE incorporated/encapsulated in nanoparticles. Although the biofilm reduction was not significant, the low concentrations used in this treatment (0.01, 0.1 and 1 mM, respectively) indicated that NCE may have some possible toxic effect against bacterial cells/biofilms, as observed in earlier experiments.

The results for treatment A and B (**Figure 30**, **Figure 31** and **Figure 32**) indicated that 37 J/cm^2 was the preferred light irradiation dose for the elimination of *S. epidermidis* biofilm in the combination with 0.01, 0.1 and 1 mM NCE. The significant reduction of intact biofilm after treatment with NCE LCNPs may be caused by the nanoparticles' overall positive surface

charge, making the biofilm matrix more susceptible for NCE, but this need to be further investigated. Since the concentration of nanoparticles was different in the different NCE LCNPs suspension, there might be a slight possibility that the number of nanoparticles on the biofilm could affect the amount of NCE reaching the bacterial cells within the biofilm. High amount of nanoparticles on the biofilm could also affect the light irradiation by preventing the light from reaching all the biofilm. There were differences in biofilm reduction between free NCE and NCE LCNPs although the differences were not always significant.

The goal of this study was to evaluate the anti-biofilm effect of NCE-mediated PDT. The optimization of biofilm elimination method resulted in many changes and alterations during the experimental period, but all the work ended in an applicable method for PDT evaluation. Our biofilm elimination method included the optimal growth of *S. epidermidis*, low concentrations of NCE (0.01, 0.1 and 1 mM, respectively), two different time intervals for pre-irradiation incubation (6 and 24 hours) and two different light irradiation doses (37 and 90 J/cm^2). Due to interesting results after the final experiments regarding significant reduction of biofilm after NCE-mediated PDT treatment, in addition to the insignificant reduction after NCE only, this method has some potential for further evaluation of anti-biofilm PDT treatment.

As we can see from the last experiment, NCE-mediated PDT has the potential to be an efficient alternative option for the treatment of *S. epidermidis* biofilm. The study was performed under limited time and there are varieties of options for optimization of the biofilm elimination approach. With an optimization of the entrapment of NCE, the NCE will be protected from the high pH of the growth media, yielding a more positively charged molecule. Optimization of the drug carrier, resulting in a more positive surface charge will provide the possibility of making bacterial cells/biofilms more susceptible to the NCE, making the NCE-mediated PDT more efficient. Several aspects regarding the NCE-mediated PDT treatment have to be further explored such as light irradiation time and doses, NCE concentrations, and exposure time of NCE. The assessment of biofilm viability before and after treatment, using resazurin staining, would be interesting to implement in the biofilm elimination method. In respect to the indications of possible NCE toxicity, an assessment of minimum efficient dose would be of interest.

6. Conclusions

Although our newly developed nanoparticles baring NCE exhibited minimal biofilm reduction, this study indicates that NCE-mediated PDT has the potential to be a new optional treatment against biofilm-forming bacteria that colonize chronic wounds. After optimization of the method for biofilm elimination in addition to the optimization of growth conditions for *S. epidermidis*, we were able to achieve reliable and reproducible results for the reduction of intact biofilm. The biofilm elimination method is based on measurements of the overall biofilm biomass after PDT treatment, making it rather easy to perform. The effect of NCE entrapped in nanoparticles was not always significant when compared to the effect achieved with free NCE, however, the use of nanoparticles as a drug carrier provides several opportunities regarding NCE stability. Further optimization of nanoparticle preparation and biofilm elimination method is necessary, and highly interesting.

7. Perspectives

Short-term perspectives

- Development and optimization of a suitable drug carrier that yields higher entrapment of NCE in addition to improved NCE stability in physiological environments
- Assessment of NCE minimum efficient dose
- Optimization of desired NCE concentrations
- Optimization of NCE exposure time
- Optimization of light irradiation time and doses
- Implementation of resazurin staining to assess biofilm viability
- Evaluation of NCE-mediated PDT against other biofilm-forming bacteria such as *Pseudomonas aeruginosa* and *Staphylococcus aureus*

Long-term perspectives

- Evaluation of elimination efficiency of biofilms formed in wounds

8. List of references

Andersen, T., Z. Vanić, G. E. Flaten, S. Mattsson, I. Tho, and N. Skalko-Basnet. 2013. "Pectosomes and Chitosomes as Delivery Systems for Metronidazole: The One-Pot Preparation Method." *Pharmaceutics* 5: 445–456.

Ausbacher, D., A. Fallarero, J. Kujala, A. Määttänen, J. Peltonen, M. B. Strøm, and P. M. Vuorela. 2014. "Staphylococcus Aureus Biofilm Susceptibility to Small and Potent β(2,2)-Amino Acid Derivatives." *Biofouling* 30: 81–93.

Baldrick, P. 2010. "The Safety of Chitosan as a Pharmaceutical Excipient." *Regulatory Toxicology and Pharmacology* 56: 290–299.

Barbieri, S., F. Sonvico, C. Como, G. Colombo, F. Zani, F. Buttini, R. Bettini, A. Rossi, and P. Colombo. 2013. "Lecithin/chitosan Controlled Release Nanopreparations of Tamoxifen Citrate: Loading, Enzyme-Trigger Release and Cell Uptake." *Journal of Controlled Release* 167: 276–283.

Baroni, A., E. Buommino, V. De Gregorio, E. Ruocco, V. Ruocco, and R. Wolf. 2012. "Structure and Function of the Epidermis Related to Barrier Properties." *Clinics in Dermatology* 30: 257–262.

Barratt, G. 1999. "Characterization of Colloidal Drug Carrier Systems with Zeta Potential." *Pharmaceutical Technology Europe* 11: 25–32.

Bechet, D., P. Couleaud, C. Frochot, M.-L. Viriot, F. Guillemin, and M. Barberi-Heyob. 2008. "Nanoparticles as Vehicles for Delivery of Photodynamic Therapy Agents." *Trends in Biotechnology* 26: 612–621.

Berger, J., M. Reist, J. M. Mayer, O. Felt, N. A. Peppas, and R. Gurny. 2004. "Structure and Interactions in Covalently and Ionically Crosslinked Chitosan Hydrogels for Biomedical Applications." *European Journal of Pharmaceutics and Biopharmaceutics* 57: 19–34.

Bhatta, R. S., H. Chandasana, Y. S. Chhonker, C. Rathi, D. Kumar, K. Mitra, and P. K. Shukla. 2012. "Mucoadhesive Nanoparticles for Prolonged Ocular Delivery of Natamycin: In Vitro and Pharmacokinetics Studies." *International Journal of Pharmaceutics* 432: 105–112.

Boateng, J. S., K. H. Matthews, H. N. E. Stevens, and G. M. Eccleston. 2008. "Wound Healing Dressings and Drug Delivery Systems : A Review." *Journal of Pharmaceutical Sciences* 97: 2892–2923.

Bouwstra, J., and M. Ponec. 2006. "The Skin Barrier in Healthy and Diseased State." *Biochimica et Biophysica Acta (BBA) - Biomembranes* 1758: 2080–2095.

Bowler, P. G. 2002. "Wound Pathophysiology, Infection and Therapeutic Options." *Annals of Medicine* 34: 419–427.

Budai, L., N. Kaszás, P. Gróf, K. Lenti, K. Maghami, I. Antal, I. Klebovich, I. Petrikovics, and M. Budai. 2013. "Liposomes for Topical Use: A Physico-Chemical Comparison of Vesicles Prepared from Egg or Soy Lecithin." *Scientia Pharmaceutica* 81: 1151–1166.

Chadha, R., S. Bhandari, D. Kataria, S. Gupta, and D. Singh Jain. 2012. "Exploring the Potential of Lecithin/chitosan Nanoparticles in Enhancement of Antihypertensive Efficacy of Hydrochlorothiazide." *Journal of Microencapsulation* 29: 805–12.

Charnock, C. 2011. "Efficacy of 5-ALA Ester PDT in the in Vitro Reduction of Staphylococcus Aureus and Pseudomonas Aeruginosa by Dose-Response Curves - PDT Effects of Three Different 5-ALA Esters." *Report for Photocure*. Oslo.

Christensen, G. D., W. A. Simpson, J. J. Younger, L. M. Baddour, F. F. Barrett, D. M. Melton, and E. H. Beachey. 1985. "Adherence of Coagulase-Negative Staphylococci to Plastic Tissue Culture Plates: A Quantitative Model for the Adherence of Staphylococci to Medical Devices." *Journal of Clinical Microbiology* 22: 996–1006.

Christensen, G. J. M., and H. Brüggemann. 2014. “Bacterial Skin Commensals and Their Role as Host Guardians.” *Beneficial Microbes* 5: 201–215.

Dai, T., B. B. Fuchs, J. J. Coleman, R. A. Prates, C. Astrakas, T. G. St Denis, M. S. Ribeiro, E. Mylonakis, M. R. Hamblin, and G. P. Tegos. 2012. “Concepts and Principles of Photodynamic Therapy as an Alternative Antifungal Discovery Platform.” *Frontiers in Microbiology* 3: 1–16.

Dai, T., Y.-Y. Huang, and M. R. Hamblin. 2009. “Photodynamic Therapy for Localized Infections-State of the Art.” *Photodiagnosis and Photodynamic Therapy* 6: 170–188.

Dai, T., M. Tanaka, Y.-Y. Huang, and M. R. Hamblin. 2011. “Chitosan Preparations for Wounds and Burns: Antimicrobial and Wound-Healing Effects.” *Expert Review of Anti-Infective Therapy* 9: 857–879.

Demidova-Rice, T. N., M. R. Hamblin, and I. M. Herman. 2012. “Acute and Impaired Wound Healing: Pathophysiology and Current Methods for Drug Delivery, Part 1: Normal and Chronic Wounds: Biology, Causes, and Approaches to Care.” *Advanced Skin Wound Care* 25: 304–314.

DUSA Pharmaceuticals. 2014. “Levulan® Kerastick®.” Accessed May 15. http://www.dusapharma.com/kerastick.html.

Edwards, R., and K. G. Harding. 2004. “Bacteria and Wound Healing.” *Current Opinion in Infectiuos Diseases* 17: 91–96.

El Maghraby, G. M., B. W. Barry, and A. C. Williams. 2008. “Liposomes and Skin: From Drug Delivery to Model Membranes.” *European Journal of Pharmaceutical Sciences* 34: 203–222.

Fotinos, N., M. A. Campo, F. Popowycz, R. Gurny, and N. Lange. 2006. “5-Aminolevulinic Acid Derivatives in Photomedicine: Characteristics, Application and Perspectives.” *Photochemistry and Photobiology* 82: 994–1015.

Frankenberg, N., J. Moser, and D. Jahn. 2003. “Bacterial Heme Biosynthesis and Its Biotechnological Application.” *Applied Microbiology and Biotechnology* 63: 115–127.

Fu, X.-J., Y. Fang, and M. Yao. 2013. “Antimicrobial Photodynamic Therapy for Methicillin-Resistant Staphylococcus Aureus Infection.” *BioMed Research International* 2013: a159157.

Hadgraft, J. 2004. “Skin Deep.” *European Journal of Pharmaceutics and Biopharmaceutics* 58: 291–299.

Hafner, A., M. Dürrigl, I. Pepić, and J. Filipović-Grčić. 2011. “Short- and Long-Term Stability of Lyophilised Melatonin-Loaded Lecithin/chitosan Nanoparticles.” *Chemical & Pharmaceutical Bulletin* 59: 1117–1123.

Hafner, A., J. Lovrić, I. Pepić, and J. Filipović-Grčić. 2011. “Lecithin/chitosan Nanoparticles for Transdermal Delivery of Melatonin.” *Journal of Microencapsulation* 28: 807–815.

Hall, M. R., E. McGillicuddy, and L. J. Kaplan. 2014. “Biofilm: Basic Principles, Pathophysiology, and Implications for Clinicians.” *Surgical Infections* 15: 1–7.

Hamblin, M. R., and T. Hasan. 2004. “Photodynamic Therapy: A New Antimicrobial Approach to Infectious Disease?” *Photochemical and Photobiological Sciences* 3: 436–450.

Hannigan, G. D., and E. A. Grice. 2013. “Microbial Ecology of the Skin in the Era of Metagenomics and Molecular Microbiology.” *Cold Spring Harbor Perspectives in Medicine* 3: a015362.

Hashimoto, M. C. E., R. A. Prates, I. T. Kato, S. C. Núñez, L. C. Courrol, and M. S. Ribeiro. 2012. “Antimicrobial Photodynamic Therapy on Drug-Resistant Pseudomonas Aeruginosa-Induced Infection. An in Vivo Study.” *Photochemistry and Photobiology* 88: 590–595.

Hwa, C., E. A. Bauer, and D. E. Cohen. 2011. “Skin Biology.” *Dermatologic Therapy* 24: 464–470.
Johnsson, A., and S. Ramstad. 2003. “PDT Effects in P.acnes Treated with ALA Esters and Red Light from Photocure’s CureLight LED 12.” *Report for Photocure*. Trondheim.
Jori, G., C. Fabris, M. Soncin, S. Ferro, O. Coppellotti, D. Dei, L. Fantetti, G. Chiti, and G. Roncucci. 2006. “Photodynamic Therapy in the Treatment of Microbial Infections: Basic Principles and Perspective Applications.” *Lasers in Surgery and Medicine* 38: 468–481.
Kennedy, J. C., and R. H. Pottier. 1992. “Endogenous Protoporphyrin IX, a Clinically Useful Photosensitizer for Photodynamic Therapy.” *Journal of Photochemistry and Photobiology B: Biology* 14: 275–292.
Kishen, A., Z. Shi, A. Shrestha, and K. G. Neoh. 2008. “An Investigation on the Antibacterial and Antibiofilm Efficacy of Cationic Nanoparticulates for Root Canal Disinfection.” *Journal of Endodontics* 34: 1515–1520.
Kong, M., X. G. Chen, K. Xing, and H. J. Park. 2010. “Antimicrobial Properties of Chitosan and Mode of Action: A State of the Art Review.” *International Journal of Food Microbiology* 144: 51–63.
Lazarus, G. S., D. M. Cooper, D. R. Knighton, D. J. Margolis, R. E. Percoraro, G. Rodeheaver, and M. C. Robson. 1994. “Definitions and Guidelines for Assessment of Wounds and Evaluation of Healing.” *Wound Repair and Regeneration* 2: 165–170.
Lee, S. H., S. K. Jeong, and S. K. Ahn. 2006. “An Update of the Defensive Barrier Function of Skin.” *Yonsei Medical Journal* 47: 293–306.
Li, X., H. Guo, Q. Tian, G. Zheng, Y. Hu, Y. Fu, and H. Tan. 2013. “Effects of 5-Aminolevulinic Acid-Mediated Photodynamic Therapy on Antibiotic-Resistant Staphylococcal Biofilm: An in Vitro Study.” *The Journal of Surgical Research* 184: 1013–1021.
Macià, M. D., E. Rojo-Molinero, and A. Oliver. 2014. “Antimicrobial Susceptibility Testing in Biofilm Growing Bacteria.” *Clinical Microbiology and Infection*. doi:10.1111/1469-0691.12651.
Martindale: The Complete Drug Reference. 2014. “Protoporphyrin IX Disodium.” Accessed May 18. http://www.medicinescomplete.com/mc/martindale/current/5575-n.htm?q=protoporphyrin&t=search&ss=text&p=1#_hit.
Menezes, P. F. C., M. B. Requena, and V. S. Bagnato. 2014. “Optimization of Photodynamic Therapy Using Negative Pressure.” *Photomedicine and Laser Surgery* 32: 1–6.
Moghadas-Sharif, N., B. S. Fazly Bazzaz, B. Khameneh, and B. Malaekeh-Nikouei. 2014. “The Effect of Nanoliposomal Formulations on Staphylococcus Epidermidis Biofilm.” *Drug Development and Industrial Pharmacy*. doi:10.3109/03639045.2013.877483.
Mohanraj, V. J., and Y. Chen. 2006. “Nanoparticles – A Review.” *Tropical Journal of Pharmaceutical Research* 5: 561–573.
Mohd Hilmi, A. B., A. S. Halim, H. Jaafar, A. B. Asiah, and A. Hassan. 2013. “Chitosan Dermal Substitute and Chitosan Skin Substitute Contribute to Accelerated Full-Thickness Wound Healing in Irradiated Rats.” *BioMed Research International* 2013: a795458.
Morley, S., J. Griffiths, G. Philips, H. Moseley, C. O’Grady, K. Mellish, C. L. Lankester, et al. 2013. “Phase IIa Randomized, Placebo-Controlled Study of Antimicrobial Photodynamic Therapy in Bacterially Colonized, Chronic Leg Ulcers and Diabetic Foot Ulcers: A New Approach to Antimicrobial Therapy.” *The British Journal of Dermatology* 168: 617–624.
Mrhar, A., S. Baumgartner, A. Hafner, J. Lovrić, D. Voinovich, and J. Filipović-Grčić. 2009. “Melatonin-Loaded Lecithin/chitosan Nanoparticles: Physicochemical Characterisation

and Permeability through Caco-2 Cell Monolayers." *International Journal of Pharmaceutics* 381: 205–213.
Nostro, A., L. Cellini, G. Ginestra, M. D'Arrigo, M. di Giulio, A. Marino, A. R. Blanco, A. Favaloro, and G. Bisignano. 2013. "Staphylococcal Biofilm Formation as Affected by Type Acidulant." *APMIS : Acta Pathologica, Microbiologica, et Immunologica Scandinavica*. doi:10.1111/apm.12210.
O'Toole, G., H. B. Kaplan, and R. Kolter. 2000. "Biofilm Formation as Microbial Development." *Annual Review of Microbiology* 54: 49–79.
Pelgrift, R. Y., and A. J. Friedman. 2013. "Nanotechnology as a Therapeutic Tool to Combat Microbial Resistance." *Advanced Drug Delivery Reviews* 65: 1803–1815.
Percival, S. L., K. E. Hill, D. W. Williams, S. J. Hooper, D. W. Thomas, and J. W. Costerton. 2012. "A Review of the Scientific Evidence for Biofilms in Wounds." *Wound Repair and Regeneration* 20: 647–657.
Pharmaceutical Excipients. 2014a. "Lecithin." Accessed May 18. http://www.medicinescomplete.com/mc/excipients/current/1001940783.htm?q=phosphatidylcholine&t=search&ss=text&p=5#_hit.
Pharmaceutical Excipients. 2014b. "Chitosan." Accessed May 19. http://www.medicinescomplete.com/mc/excipients/current/1001936100.htm?q=chitosan&t=search&ss=text&p=1#_hit.
Porcheron, G., A. Garénaux, J. Proulx, M. Sabri, and C. M. Dozois. 2013. "Iron, Copper, Zinc, and Manganese Transport and Regulation in Pathogenic Enterobacteria: Correlations between Strains, Site of Infection and the Relative Importance of the Different Metal Transport Systems for Virulence." *Frontiers in Cellular and Infection Microbiology* 3: 1–24.
Proksch, E., J. M. Brandner, and J.-M. Jensen. 2008. "The Skin: An Indispensable Barrier." *Experimental Dermatology* 17: 1063–1072.
Redmond, R. W., and J. N. Gamlin. 1999. "Invited Review A Compilation of Singlet Oxygen Yields from Biologically Relevant Molecules." *Photochemistry and Photobiology* 70: 391–475.
Reinke, J. M., and H. Sorg. 2012. "Wound Repair and Regeneration." *European Surgical Research* 49: 35–43.
Rolfe, M. D., C. J. Rice, S. Lucchini, C. Pin, A. Thompson, A. D. S. Cameron, M. Alston, et al. 2012. "Lag Phase Is a Distinct Growth Phase That Prepares Bacteria for Exponential Growth and Involves Transient Metal Accumulation." *Journal of Bacteriology* 194: 686–701.
Rosso, J. Q. Del, and K. Cash. 2013. "Topical Corticosteroid Application and the Structural and Functional Integrity of the Epidermal Barrier." *Journal of Clinical Aesthetic Dermatology* 6: 20–27.
Sambrook, J. F., and D. W. Russell. 2001. *Molecular Cloning: A Laboratory Manual, Volume 3*. 3rd ed. New York: Cold Spring Harbor Laboratory Press.
Sanford, J. A., and R. L. Gallo. 2013. "Functions of the Skin Microbiota in Health and Disease." *Seminars in Immunology* 25: 370–377.
Senyiğit, T., F. Sonvico, S. Barbieri, O. Ozer, P. Santi, and P. Colombo. 2010. "Lecithin/chitosan Nanoparticles of Clobetasol-17-Propionate Capable of Accumulation in Pig Skin." *Journal of Controlled Release* 142: 368–763.
Sharma, S. K., P. Mroz, T. Dai, Y.-Y. Huang, T. G. St Denis, and M. R. Hamblin. 2012. "Photodynamic Therapy for Cancer and for Infections: What Is the Difference?" *Israel Journal of Chemistry* 52: 691–705.
Shaw, T. J., and P. Martin. 2009. "Wound Repair at a Glance." *Journal of Cell Science* 122: 3209–3213.

Sherwood, L. 2010. *Human Physiology: From Cells to Systems*. 7th ed. Australia: Thomson Brooks Cole.

Shrestha, A., M. R. Hamblin, and A. Kishen. 2014. "Photoactivated Rose Bengal Functionalized Chitosan Nanoparticles Produce Antibacterial/biofilm Activity and Stabilize Dentin-Collagen." *Nanomedicine : Nanotechnology, Biology, and Medicine* 10: 491–501.

Simonetti, O., O. Cirioni, F. Orlando, C. Alongi, G. Lucarini, C. Silvestri, A. Zizzi, et al. 2011. "Effectiveness of Antimicrobial Photodynamic Therapy with a Single Treatment of RLP068/Cl in an Experimental Model of Staphylococcus Aureus Wound Infection." *British Journal of Dermatology* 164: 987–995.

Singh, M. R., S. Saraf, A. Vyas, V. Jain, and D. Singh. 2013. "Innovative Approaches in Wound Healing: Trajectory and Advances." *Artificial Cells, Nanomedicine, and Biotechnology* 41: 202–212.

Sonvico, F., A. Cagnani, A. Rossi, S. Motta, M. T. Di Bari, F. Cavatorta, M. J. Alonso, A. Deriu, and P. Colombo. 2006. "Formation of Self-Organized Nanoparticles by Lecithin/chitosan Ionic Interaction." *International Journal of Pharmaceutics* 324: 67–73.

St Denis, T. G., T. Dai, L. Izikson, C. Astrakas, R. R. Anderson, M. R. Hamblin, and G. P. Tegos. 2011. "All You Need Is Light - Antimicrobial Photoinactivation as an Evolving and Emerging Discovery Strategy against Infectious Disease." *Virulence* 2: 509–520.

Stepanović, S., D. Vuković, P. Jezek, M. Pavlović, and M. Svabic-Vlahović. 2001. "Influence of Dynamic Conditions on Biofilm Formation by Staphylococci." *European Journal of Clinical Microbiology & Infectious Diseases* 20: 502–4.

Tan, A., A. M. Seifalian, A. Gupta, P. Avci, M. Sadasivam, R. Chandran, N. Parizotto, et al. 2013. "Shining Light on Nanotechnology to Help Repair and Regeneration." *Biotechnology Advances* 31: 607–631.

Tan, Q., W. Liu, C. Guo, and G. Zhai. 2011. "Preparation and Evaluation of Quercetin-Loaded Lecithin-Chitosan Nanoparticles for Topical Delivery." *International Journal of Nanomedicine* 6: 1621–1630.

Tanaka, M., M. Kinoshita, Y. Yoshihara, N. Shinomiya, S. Seki, K. Nemoto, T. Hirayama, et al. 2012. "Optimal Photosensitizers for Photodynamic Therapy of Infections Should Kill Bacteria but Spare Neutrophils." *Photochemistry and Photobiology* 88: 227–232.

Taraszkiewicz, A., G. Fila, M. Grinholc, and J. Nakonieczna. 2012. "Innovative Strategies to Overcome Biofilm Resistance." *BioMed Research International* 2013: a150653.

Thomson, C. H. 2011. "Biofilms: Do They Affect Wound Healing?" *International Wound Journal* 8: 63–67.

Van den Driessche, F., P. Rigole, G. Brackman, and T. Coenye. 2014. "Optimization of Resazurin-Based Viability Staining for Quantification of Microbial Biofilms." *Journal of Microbiological Methods* 98: 31–34.

Vecchio, D., T. Dai, L. Huang, L. Fantetti, G. Roncucci, and M. R. Hamblin. 2013. "Antimicrobial Photodynamic Therapy with RLP068 Kills Methicillin-Resistant Staphylococcus Aureus and Improves Wound Healing in a Mouse Model of Infected Skin Abrasion." *Journal of Biophotonics* 6: 733–742.

Wachowska, M., A. Muchowicz, M. Firczuk, M. Gabrysiak, M. Winiarska, M. Wańczyk, K. Bojarczuk, and J. Golab. 2011. "Aminolevulinic Acid (ALA) as a Prodrug in Photodynamic Therapy of Cancer." *Molecules* 16: 4140–4164.

Wild, T., A. Rahbarnia, M. Kellner, L. Sobotka, and T. Eberlein. 2010. "Basics in Nutrition and Wound Healing." *Nutrition* 26: 862–866.

Wong, T. W. 2009. "Chitosan and Its Use in Design of Insulin Delivery System." *Recent Patents on Drug Delivery & Formulation* 3: 8–25.

Zhang, A., H. Mu, W. Zhang, G. Cui, J. Zhu, and J. Duan. 2013. “Chitosan Coupling Makes Microbial Biofilms Susceptible to Antibiotics.” *Scientific Reports* 3. doi:10.1038/srep03364.

Özcan, I., E. Azizoğlu, T. Senyiğit, M. Özyazici, and Ö. Özer. 2013. “Comparison of PLGA and Lecithin/chitosan Nanoparticles for Dermal Targeting of Betamethasone Valerate.” *Journal of Drug Targeting* 21: 542–50.

Özcan, I., E. Azizoğlu, T. Senyiğit, M. Özyazıcı, and Ö. Özer. 2013. “Enhanced Dermal Delivery of Diflucortolone Valerate Using Lecithin/chitosan Nanoparticles: In-Vitro and in-Vivo Evaluations.” *International Journal of Nanomedicine* 8: 461–475.